Deep-water syn-rift stratigraphy as archives of Early-Mid Pleistocene palaeoenvironmental signals and controls on sediment delivery

Timothy M. Cullen*[1,2], Richard E. Ll. Collier[1], David M. Hodgson[1], Robert L. Gawthorpe[2], Katerina Kouli[3], Marco Maffione[4], Haralambos Kranis [3], Gauti T. Eliassen[2].

1. School of Earth and Environment, University of Leeds, Leeds, United Kingdom
2. Department of Earth Sciences, University of Bergen, Bergen, Norway (*tim.cullen@uib.no)
3. Department of Geology and Geoenvironment, National and Kapodistrian University of Athens, Athens, Greece
4. Department of Earth and Environmental Sciences, University of Birmingham, Birmingham, United Kingdom

---

Abstract

The timing and character of coarse siliciclastic sediment delivered to deep-water environments in active rift basins is governed by the complicated interactions of tectonics, climate, eustasy, hinterland geology, and shelf process regime. The stratigraphic archives of deep-water syn-rift basin-fills provide records of palaeoenvironmental changes (e.g. climate and vegetation) in onshore catchments, particularly where they are connected by narrow shelves. However, a chronostratigraphically constrained record of climatic fluctuations and process responses in the hinterland source area recorded in deep-water deposits is rare. Here, we integrate a fully cored research borehole with outcrop exposures of deep-water syn-rift stratigraphy to reconstruct palaeoenvironmental change within the stratigraphy of the West Xylokastro Fault Block in the Corinth Rift, Greece. We used palaeomagnetic and palynological analyses from borehole core samples to develop a chronostratigraphic and palaeoenvironmental model, which we compare to global records of Early-Mid Pleistocene climate and eustatic change. This framework allows establishment of a chronostratigraphic and palaeoenvironmental context to stratigraphic variability encountered in outcrop and in the borehole. Our results show that the ~240 m thick studied succession was deposited from ~1.1 to 0.6 Ma across the Early- to Mid-Pleistocene transition. During the Early Pleistocene, obliquity-paced climatic variability is largely coherent with vegetation changes of forest coverage within catchments on the southern margin of the Corinth Rift. Large magnitude, eccentricity-paced cyclicity dominant after the Mid-Pleistocene Transition can alter sediment supply from onshore catchments during the warming stages of severe interglacials where expansion of forest cover traps sediment within catchments. Conglomeratic grade sediment delivery to the deep-water is enhanced during glacial periods, interpreted to reflect sparse forest cover and large winter storms, and during semi-arid, grassland-dominated interglacial highstands during severe interglacials. Base-level rise during minor interglacials is easily outpaced by high sediment supply and is seldom represented stratigraphically. The study demonstrates the value of integrated palynological and sedimentological studies, whilst applying a conservative approach to interpretation when dealing with sparse palynological records from proximal deep-water stratigraphy. The case study provides conceptual models where climatic and vegetation changes can begin to be incorporated as a key control on sediment flux from onshore drainage basins to deep-water syn-rift successions.

1 Introduction

Deep-water, syn-rift depositional systems are highly dynamic. Short-scale temporal and spatial changes in accommodation produce complicated depocenters that can receive substantial but variable coarse-grained sediment supply on account of steep gradients, short transport distances and multiple input systems (Gawthorpe et al., 1994; Hadler-Jacobsen et al., 2005; Pechlivanidou et al., 2019). Despite this well-known complexity, smaller scale variability of deep-water syn-rift systems attributable to palaeoenvironmental change are seldom considered in depositional models, especially in comparison to responses to tectonic forcing, or eustatic variability in shallow water systems (e.g. Collier, 1990; Muravchik et al., 2017; Gawthorpe et al., 2017). Deep-water syn-rift systems are often directly linked to terrestrial drainage catchments as rift-basin physiography does not favour the development of wide shelves, and instead produces steep, short source-to-sink configurations (Gawthorpe et al., 1994; Sømme et al., 2009; Hadler-Jacobsen et al., 2005; Nelson et al., 2009; Covault & Graham, 2010; Armitage et al., 2013; Nyberg et al., 2018). As a result, sediment supply variability to the deep-water does not necessarily follow 'classical' lowstand or falling base-level models (Posamentier & Vail, 1988; Hadler-Jacobsen et al., 2005; Sømme et al., 2009; Nelson et al., 2009; Strachan et al., 2013; Watkins et al., 2018; Zhang et al., 2019a, b) and shelf process regime is less influential or can be considered fluvially-driven (Dixon et al., 2012; Cosgrove et al., 2018). Consequently, changes in sediment flux within onshore drainage catchments should have direct implications for deep-water sediment delivery (Collier et al., 2000; Blum & Hattier-Womack, 2009; Armitage et al., 2011; Romans et al., 2016; Watkins et al., 2018; Sømme et al., 2019; Tofelde et al., 2021). Although changes in sedimentation rate in deep-water syn-rift depositional systems are recognised or interpreted (Guiterrez-Pastor et al., 2009; Nelson et al., 2009; Pechlivanidou et al., 2018; McNeil et al., 2019a), the interplay of external factors that control changes in sediment flux are seldom well constrained. Changes in climate are a fundamental control on sediment flux from drainage catchments, either through changes in precipitation patterns or magnitude, or through resultant changes in catchment character such as vegetation (Leeder et al., 1998; Collier et al., 2000; Bogaart et al., 2002). However, the way these factors interact to govern sediment flux to the deep-water, and how confidently they can be inverted from stratigraphy remains unclear.

Environmental signals are defined by Tofelde et al., (2021) as '*a measurable change in any sedimentary parameter of interest through time that can be linked to an environmental change*'. However, the record of environmental signals resulting from changes in catchment sediment flux in deep-water stratigraphy can be complicated by sediment transport processes or buffered by transient, up-dip storage (Jerolmack & Paola, 2010; Simpson & Castellort, 2012; Armitage et al., 2013; Watkins et al., 2018; Staub et al., 2020). The growth and death of extensional faults can additionally impact sediment routing patterns, and either inhibit or promote siliciclastic delivery to the deep-water (Gupta et al., 1999; Nelson et al., 2009; Gawthorpe et al., 2018; Geurts et al., 2018; Pechlivanidou et al., 2019). Typically, tectonic changes operate on 10^5-10^6 yr timescales (e.g. Allen et al., 2008; Romans et al., 2016, Ford et al., 2016; Gawthorpe et al., 2018), whereas climatic variability can be identified on higher order, 10^4-10^5 yr timescales (e.g. Collier et al., 2000; Nelson et al., 2009; Allen et al., 2008; Blum & Hattier-Womack, 2009; Watkins et al., 2018; Sømme et al., 2019). The overlap in the timescales for these controls makes determining relative influences of climate and tectonics on stratigraphy challenging, especially in under-filled deep-water basins (Allen et al., 2008; Whittaker et al., 2010, 2011; Armitage et al., 2011; Romans et al., 2016; Sømme et al., 2019). The difficulty of confident palaeoenvironmental reconstruction, against comparatively more accessible and certain structural mapping, may mean that many depositional models tend to favour tectonics as a principal driving force, even at 10^4-10^5 yr timescales. However, numerical modelling and quantitative sediment volume reconstructions have demonstrated that non-tectonic sediment supply variability has the potential to dramatically alter the stratigraphy within rift basin-fills, and this complexity should be included in conceptual models for deep-water syn-rift systems (Leeder et al., 1998; Collier et al., 2000; Barrett et al., 2017; Armitage et al., 2018; Watkins et al., 2018; Tofelde et al., 2021).

Climate and related changes in vegetation impart a major control on sedimentary parameters (e.g. grain size and shape), and the extent and duration of sediment erosion and transport (Leeder et al., 1998; Collier et al., 2000; Blum & Hattier-Womack, 2009; Kneller et al., 2009; Nelson et al., 2009; Bourget et al., 2010a,b; Armitage et al., 2011; Watkins et al., 2018, McNeil et al., 2019a). However, the dynamic response of catchments to climatic change is poorly understood and difficult to reconstruct (Cordier et al., 2017). Climatic modelling (Leeder et al., 1998; Armitage et al., 2011, 2013), eroded and offshore sediment volumes (Collier et al. 2000; Watkins et al., 2018), and drainage modelling (Pechlivanidou et al., 2019) highlight diverse climatic regimes and drainage configurations in rift catchments. As a result, the potential mechanisms for variable sediment production and carrying capacity are extremely broad. The role of vegetation as a control on sediment flux to the deep-water is largely unexplored beyond numerical models (Leeder et al., 1998; Schmid et al., 2018) with relatively few paired examples where the source-to-sink configuration can be confidently constrained (Collier et al., 2000; Sømme et al., 2011; Cheng et al., 2017).

Here, we use exposures and a fully cored research borehole to identify the palaeoenvironmental controls on sediment flux to an exhumed, Early-Mid Pleistocene, deep-water system, in the West Xylokastro Fault Block (WXFB) of the Corinth Rift, Greece. Climatic fluctuations in the Corinth Rift through the Pleistocene and Holocene are well documented (Collier et al., 2000; Watkins et al., 2018; Barrett et al., 2019; McNeil et al., 2019a), although contrasting interpretations of glacial- (Collier et al., 2000) or interglacial-dominated (Watkins et al., 2018) sediment supply to the deep-water have been suggested. Stratigraphic correlations permit the architectures observed in the up-dip, fan delta feeder system to be tied to palynological palaeoenvironmental proxies in the deep-water stratigraphy using an age model generated through palaeomagnetic and tectonostratigraphic methods. This is compared with other Corinthian and Mediterranean climatic records and deposits in order to 1) test the reliability of complex, non-ideal, deep-water stratigraphic successions as records for Quaternary environmental change, 2) investigate the response of the deep-water syn-rift systems to Quaternary climatic and vegetation variability on 10^4-10^5 yr timescales, and 3) propose new conceptual models for palaeoenvironmental controls on sediment supply to ancient deep-water syn-rift systems.

2 Geological Setting

The Corinth Rift is an active E-W-striking basin initiated ~5 Ma in response to NNE-SSW extension associated with the subduction and roll-back of the African plate beneath the European and Anatolian plates (Doutsos & Poulimenos, 1992; Collier & Dart, 1991; Armijo, 1996; Leeder et al., 2003; McNeil et al., 2005; Bell et al., 2009; Skourtsos & Kranis, 2009; Taylor et al., 2011; Beckers et al., 2015; Nixon et al., 2016). In the study area (Figure 1), the uppermost pre-rift stratigraphy is represented by a ~1.3 km thick succession of Mesozoic carbonates and Cenozoic siliciclastics arranged in ~N-S-striking, west-verging thrust sheets related to the Hellanide thrust belt (Piper, 2006; Skourtsos & Kranis, 2009; Ford et al., 2013; Skourtsos et al., 2016; Gawthorpe et al., 2018). Gawthorpe et al. (2018) subdivided the syn-rift stratigraphy of the southern margin into two main phases: i) Rift 1, 5.0-3.6 to 2.2-1.8 Ma, within dispersed, localised depocentres filled by early syn-rift alluvial and fluvial deposits, with a younger Gilbert-type fan delta and deep-water component, and ii) Rift 2, 2.2-1.8 Ma to the present day, which comprises localised, but partially connected, depocentres with Gilbert-type fan deltas and associated deep-water deposits (Collier & Dart, 1991; Rohais et al., 2008; Backert et al., 2010; Gobo et al., 2014; Barrett et al., 2019; Gawthorpe et al., 2018; Muravchik et al., 2020; Cullen et al., 2020). The Rethi-Dendro Formation (RDF – Leeder et al., 2012) of the Rift 2 phase is exposed in the West Xylokastro Fault Block (WXFB) on the southern margin of the Gulf of Corinth (Figure 1). The WXFB is a ~12 km long, 6-8 km wide fault terrace bound by the E-W-trending West Xylokastro Fault to the south, and the E-W Derveni and NW-SE-trending Lykoporiá Faults to the north (Figure 1). The RDF in the study area comprises an axial, delta-derived system, and a transverse fault-scarp apron system (Gawthorpe et al., 2018; Cullen et al., 2020). Palaeocurrents and the inclusion of metamorphic clasts indicate the main source of sediment input is from the Ilias fan delta fed by the well-established Olvios drainage catchment (Rohais et al., 2007a; Gobo et al., 2014, 2015; Rohais & Moretti, 2017; Rubi et al., 2018; Gawthorpe et al., 2018; Zhong et al., 2018; Cullen et al., 2020; Figure 1). An age of ~1.5 Ma – 0.7 Ma is established for the West Xylokastro RDF stratigraphy but is limited by low biostratigraphic resolution internally (Ford et al., 2016; Gawthorpe et al., 2018). Early-Mid Pleistocene palaeogeographies of the Olvios catchment indicate approximately 1600 m of elevation difference from the uppermost hinterland of Mavron Oros to the topsets and shoreline of the Ilias fan delta over a distance of ~15-18 km (Figure 1b, Gawthorpe et al., 2018, de Gelder et al., 2019).

Ilias fan delta foreset heights indicate that water-depth at the western end of the WXFB was >300-400 m, likely increasing to ~500-600 m in the centre of the fault segment demonstrated through the elevation difference and basinward thickness increases in equivalent stratigraphy(Rohais et al., 2007; Gobo et al., 2014, 2015; Ford et al., 2016; Gawthorpe et al., 2018; Rubi et al., 2018; Zhong et al., 2018; Cullen et al., 2020). Depths of this magnitude place the delta bottomsets and downdip fan well below typical storm-wave base and therefore their classification within a deep-water system. Topset radii of the Ilias fan delta are difficult to constrain due to faulted stratigraphy and later erosion, but exposures suggest they were likely <3.5 km (Rohais et al., 2007a,b, 2008; Rubi et al., 2018; Zhong et al., 2018; Cullen et al., 2020), similar to modern fan deltas along the southern shoreline. Key surfaces that can be traced in the field, combined with stratigraphic observations of lithology and sedimentology, define a stratigraphic framework subdivided into the Lower WX and the Upper WX, described in detail in Cullen et al. (2020) (Figure 1). This study focuses on the Lower WX, which is subdivided into WX1-WX7 based on lithology and key stratigraphic surfaces (Figures 1 to 4, Cullen et al., 2020). The G4 borehole (Figure 1, 2), drilled in January 2018 as part of the Syn-Rift Systems project, is situated within the basin-floor domain, 3 km from the West Xylokastro Fault and ~6 km downdip of the Ilias fan delta (Cullen et al., 2020; Figure 1). The borehole intersects 172 m of RDF stratigraphy, mostly of the axial depositional system in the hangingwall of the West Xylokastro Fault.

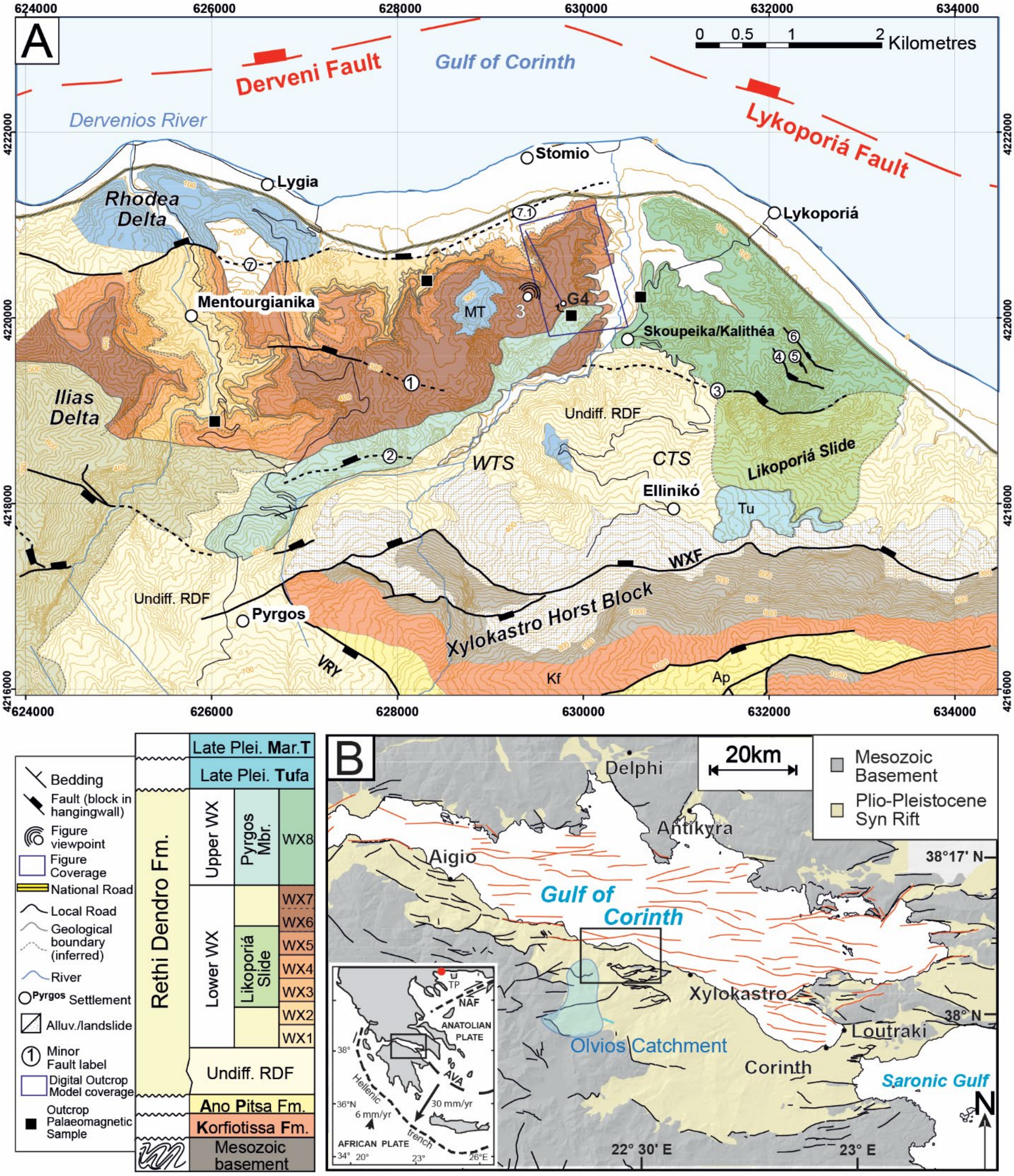

Figure 1 (previous page): A) Geological location map for the study area, the West Xylokastro fault block, modified from Cullen et al. (2020). Coordinates are UTM (in Metres) for zone 34N. MT = Marine Terrace.. Stratigraphic key for the map shows colours and relative ages of mapped units. TKF = Trikala Fault, SF=Sythas Fault, AF=Amphithea Fault, KF = Kyllini Fault, MF = Mavro Fault, WXF = West Xylokastro Fault, LF = Lykoporiá Fault, K = Kyllini, M = Mavro, E/I= Evrostini/Ilias, PM = Pyrgos Member, LS = Lykoporiá Slide VRY = Vrysoulous Fault. WTS – Western Transverse system, CTS – Central Transverse system. B) Location of the study area within the Gulf of Corinth, Central Greece highlighting the distribution of Pre-Rift and Syn-Rift stratigraphy. All mapping constructed and modified from Gawthorpe et al. 2017, compiled from Ford et al., 2013, Ford et al., 2016, Nixon et al., 2016, Skourtsos unpb. and author's own mapping. TP – Tenagi Philippon. Black box indicates the locale focused on in this paper.NAF – North Anatolian Fault. AVA – Aegean Volcanic Arc.

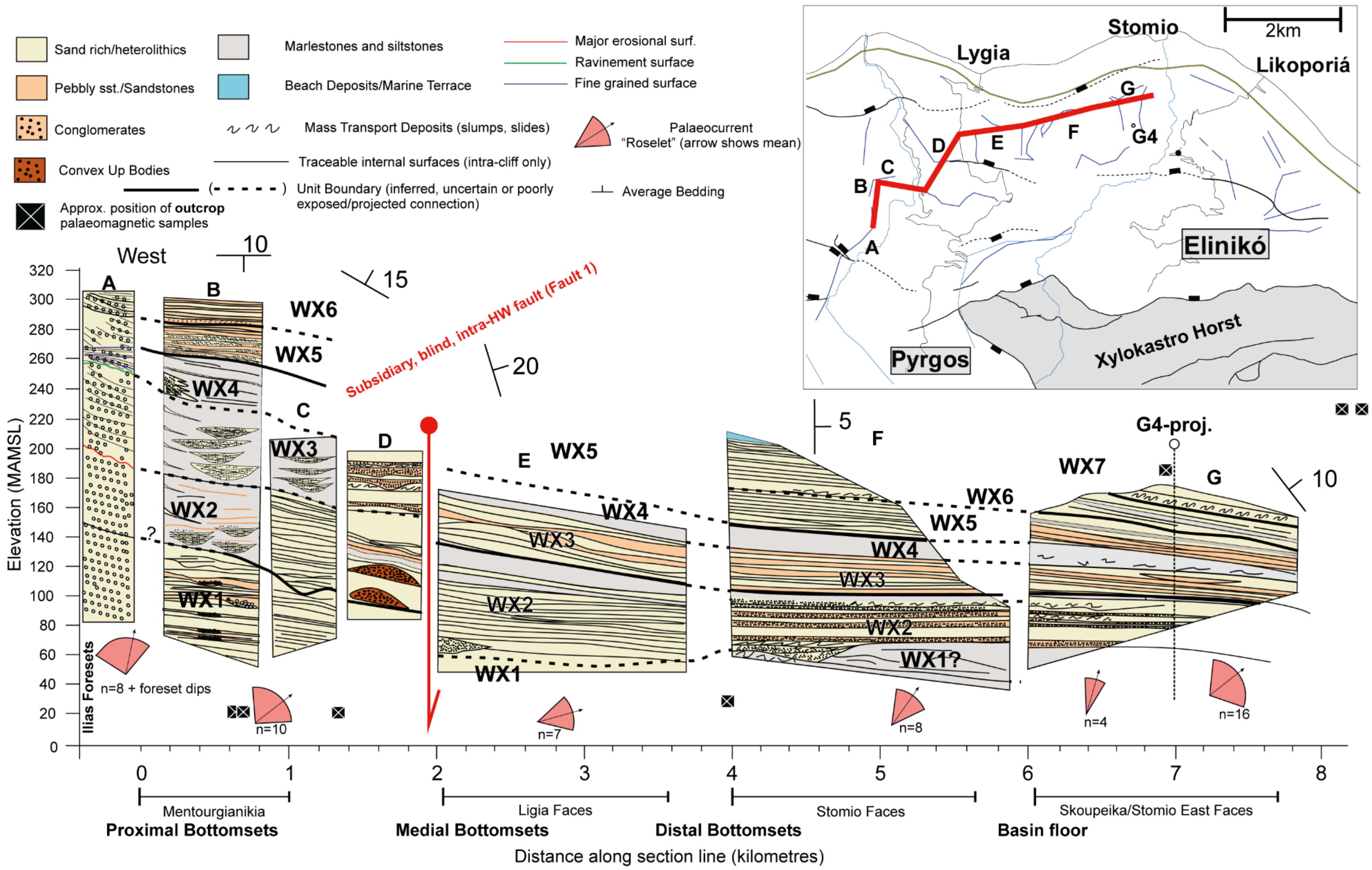

Figure 2 (next page): Summary stratigraphic correlation modified from Cullen et al. (2020) highlighting the position of the G4 borehole and outcrop samples ~ 7km downdip of the base of the Ilias delta and the supporting outcrop palaeomagnetic samples (black squares) outboard and within the G4 stratigraphy.

3 Methodology

3.1 Outcrop and core sedimentology

The G4 research borehole located near Skoupéika/Kalithea (Figure 1) retrieved a 172 m cored section, which is integrated with outcrop logging and digital outcrop models. 87% of the core showed good or excellent recovery. The stratigraphy for the West Xylokastro Fault Block RDF was developed through conventional stratigraphic and structural mapping supported by digital outcrop models outlined in Cullen et al. (2020). The G4 borehole core was logged at 1:50 scale in Greece prior to splitting and the collection of palynological and palaeomagnetic samples from the core. The core was then logged in greater detail (1:10) to provide a detailed sedimentological record to aid with the positioning of stratigraphic horizons and complement palaeoenvironmental and chronostratigraphic analysis.

3.2 Digital outcrops

The digital outcrop model for the Skoupéika exposures was generated using photographs from DJI Mavic Pro and DJI Phantom 3 Uncrewed Aerial Vehicles, with photogrammetric models built using Agisoft Photoscan Pro (now Agisoft Metashape) with interpretation in LIME (Buckley et al., 2019). Multiple orthogonal and oblique photographs were used to maximise coverage and resolution of the model. The inaccessibility of much of the outcrop meant that ground-control points were not available but consistency within the model was checked through control points compared against topographic maps of the outcrop area. Field-based stratigraphic correlations (Cullen et al., 2020) were mapped onto the model as horizons. The 3D nature of the exposure permits confident dip projections of surfaces to the wellbore, initially as an unconstrained dip projection, then constrained with greater confidence by "well-top" interpretations from core logging (Figure 3, 4, Supplementary Information 3).

Figure 3 (next page): A) The Skoupéika digital outcrop model with the projection and measurement of unit thicknesses in to the G4 borehole (Figure 5-4). Bracketed numbers indicate minimum thickness at digital log locations where a unit is constrained by the base or top of the exposure. * and ** indicate thicknesses which are projected from downdip digital logs 150 m away in the Skoupéika North Face. B) Outcrop photograph of the face in A, highlighting stratigraphic architectures and exposure of G4 stratigraphy nearby. C) Summary of the stratigraphic position of samples within, and outboard of the well stratigraphy along with unit projections. The channel body and MTD are considered within WX7

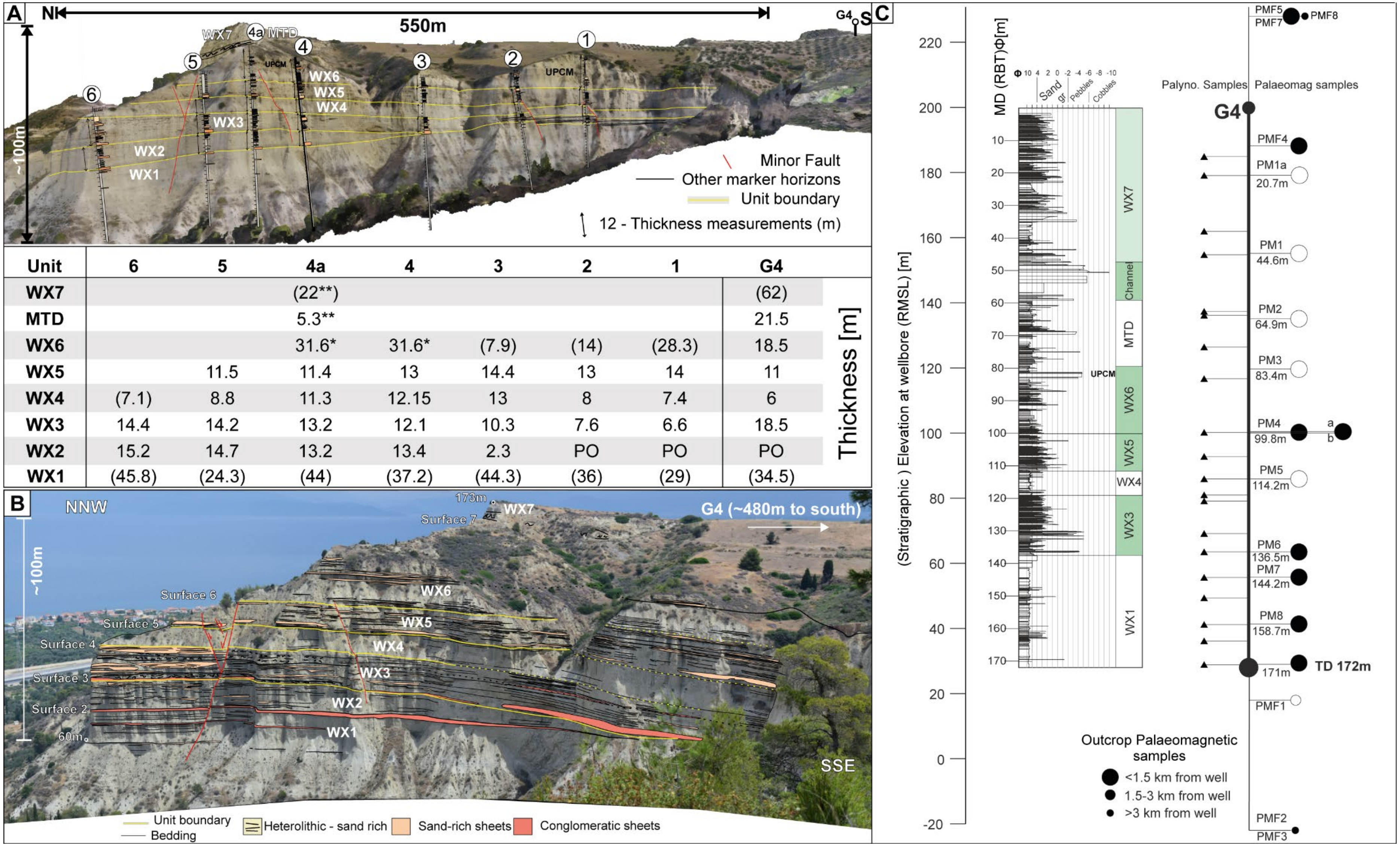

Unit	6	5	4a	4	3	2	1	G4
WX7			(22**)					(62)
MTD			5.3**					21.5
WX6			31.6*	31.6*	(7.9)	(14)	(28.3)	18.5
WX5		11.5	11.4	13	14.4	13	14	11
WX4	(7.1)	8.8	11.3	12.15	13	8	7.4	6
WX3	14.4	14.2	13.2	12.1	10.3	7.6	6.6	18.5
WX2	15.2	14.7	13.2	13.4	2.3	PO	PO	PO
WX1	(45.8)	(24.3)	(44)	(37.2)	(44.3)	(36)	(29)	(34.5)

3.3 Palaeomagnetic analysis

Seventeen samples were collected for palaeomagnetic analysis, preferentially from mudstones approximately every 20 m +/- 1 m in the core and, where available, from outcrops (Supplementary Data 1, 2). Samples were cut into 8 cm^3 cubes marked with a way up indicator from the vertical well, or vertically aligned way-up arrows from outcrop samples, where bedding never exceeded a dip of 20°. The samples were then subject to alternating field (AF) demagnetisation with an AGICO LDA5 AF demagnetiser using 12-14 AF increments from 5 to 120 mT. Natural remanent magnetization and remanence after each demagnetization step were measured with an AGICO JR5 spinner magnetometer at the PUMA Rock Magnetic laboratory, University of Birmingham. Demagnetization data were plotted on orthogonal (Zijderveld) diagrams, and the remanence components were calculated through principal component analysis (Kirschvink, 1980) using online software paleomagnetism.org (Koymans et al., 2016) (Supplementary Data 1, 2). Sample depths and locations are summarised in Figure 2 and 3 and the supplementary information. The inclinations of the isolated characteristic remanent magnetization (ChRM) were used to produce a magnetostratigraphy, which was then compared to the Geomagnetic Polarity Time Scale (Cande & Kent, 1995; Cohen & Gibbard, 2016) to produce an age model for the studied stratigraphic intervals.

3.4 Palynology

Palynology samples were collected from core every ~10 m with slight deviations to achieve good quality sample material (Supplementary Material 1,4). Intact, mudstones were preferentially sampled in order to achieve the greatest likelihood of the preservation of undamaged organic material (Paropkari et al., 1992; McNeil et al., 2019c). Samples were prepared using the method of Vidal (1988). Samples were dried at 50° C, weighed then crushed and spiked with a *Lycopodium* tablet and minor amount of distilled water to cover the sample. 20% hydrochloric acid (HCl) was then added until the reaction had ceased and was topped up with water and left to settle for at least 12 hours. The supernatant liquid was then sieved through a 10 µm cloth sieve and returned to the beaker. 50 ml of 40% hydrofluoric acid (HF) was then added and stirred and left for 48 hours. This was neutralised by topping up and sieving with water prior to simmering in 20% hydrochloric acid to remove precipitates. This solution was then re-sieved with distilled water to bring to neutral. Where precipitates remained, HCl or HF stages were repeated until all precipitates were removed before mounting on slides in glycerine jelly.

In total, 20 samples were counted for pollen, dinoflagellates and other sedimentary organic matter using a Leica DM500 light microscope at 400-630x magnification. Pollen grain and dinoflagellate cyst identification was based on Chester & Raine (2001), Beug (2015) and Mudie et al. (2017). Sedimentary Organic Matter (SOM) is grouped into three, broad categories; Amorphous Organic Matter (AOM); Non-Terrestrial Palynomorphs (NTP) comprising marine algae, acritarchs and zoomorphs (foraminiferal test linings); and Terrestrial Palynomorphs (TP) comprising freshwater algae (*Botryococcus)*, cuticle and unstructured phytoclasts, resin, degraded wood, dark structureless organic matter (DSOM) and bladed and equant organic debris (Tyson, 1996, McArthur et al., 2016a, b). All types of non-palynomorph organic matter were counted to a minimum of 300 in the classification of McArthur et al. (2016a, b).

Dinoflagellate cyst counts vary considerably and a minimum count criterion for some samples could be met with mean count of 34 (varying from 1 to 212). Most pollen samples were counted until at least 250 grains to exceed the ranges typical for validity in Quaternary lacustrine studies (Djamali & Cilleros, 2020). However, four samples were deemed barren for pollen, dinoflagellates and spores, with an additional sample showing a very low count and poor preservation of material (Supplementary Data 4). Pollen percentages for vegetation groups were calculated based on a pollen sum excluding i) Pinaceae, which are variably over-represented through the stratigraphy due to their long-distance transport (*sensu* Szczepanek et al., 2017), and ii) aquatics, due to their potential for different transport mechanisms (Beaudouin et al., 2007). For both pollen and dinoflagellates, concentrations were calculated using the *Lycopodium* exotic marker method (Supplementary Data 4) established by Benninghoff (1962) and Stockmarr (1971) and summarised in Mertens et al. (2012b) and Nguyen et al. (2013). The average pollen concentration was 577.9 grains/gram of sediment (Supplementary Data 4) ranging from 2294 grains/gram to 65.9 grains/gram for countable samples; barren samples showed between 0 - 20.7 grains/gram.

To allow for cross-comparison between age-equivalent pollen records published in the area, pollen data were also grouped (Figure 10) following the grouping of Joannin et al. (2007a, b, 2008). As in Joannin et al. (2007b, 2008) *Quercus ilex type*, *Phillyrea* and undifferentiated *Oleaceae/Olea* are treated as a Mediterranean Elements sum, and separately from deciduous trees/mesothermic elements due to their local importance. Given their potential importance in highlighting semiaquatic grass populations, *Phragmites* sp. are distinguished from the rest of Poaceae based on their typically smaller size (<27 µm) than other grains of the family (Chester & Raine, 2001). It is acknowledged that local or seasonal variability may produce unavoidable false-positive identification of *Phragmites* sp. In this case, the low concentrations *Phragmites sp.* and high concentrations of Poaceae means the impact of this on the total “Grasses” population is negligible.

In addition, ‘biomization’ (Prentice et al., 1996) allows a semi-quantitative comparison of the pollen data from this study to newer Mediterranean vegetation biome schemes. Here, we use the plant functional types and biomes of Marinova et al. (2018) derived for the Eastern Mediterranean and Southern Balkans supplemented with the plant functional types of Panagiotopoulous et al. (2020) for *Tsuga* to produce biome affinities for the following biomes (Supplementary Information 5):

- Tundra (TUND)
- Desert (DESE)
- Graminoids with Forbs (GRAM)
- Xeric Shrubland (XSHB)
- Warm-termperate evergreen sclerophyll broadleaf shrubland (WTSHB)
- Cool/Cold evergreen needleleaf forest (COOL/CENF)
- Warm-temperate/Temperate deciduous malcophyll broadleaf forest (WTDF/TEDE)
- Cool-mixed evergreen needleleaf and deciduous broadleaf forest (CMIX)
- Warm-temperate evergreen needle and sclerophyll broadleaf forest (WTEF)
- Evergreen needleleaf woodland (ENWD)

- Deciduous broadleaf woodland (DBWD)

To determine the affinity of a given assemblage, pollen taxa are organised into ‘plant functional types’ (PFTs) and arranged into a taxon x PFT matrix. Marinova et al. (2018) provide data to support the transformation of a taxon x PFT matrix to a taxon x biome matrix to establish an association between a given taxa, and a vegetation biome. Using these matrices and the approach of Prentice et al. (1996), an affinity score for a pollen sample is generated for each biome (Supplementary Information 5). The pollen sum used for the biomization does not exclude Pinaceae to not artificially reduce or enhance the affinity towards certain biomes. The square-root operation stabilizes variance and increases the methods sensitivity to less abundant taxa such that the variable over-representation of Pinaceae is accounted for (Prentice et al., 1996).

4 Stratigraphy and Outcrop-Borehole Correlation

The West Xylokastro RDF comprises seven units (WX1-7), bound by key stratal surfaces that are traced from the Ilias fan delta foresets, over 8 km downdip into the deep-water basin floor stratigraphy at the G4 borehole (Cullen et al., 2020). In this study we present the results of the correlation of the West Xylokastro Stratigraphy to the G4 borehole. Figures 3 and 4 highlight the stratigraphy in the region surrounding the G4 borehole and the lateral variability, showing 10-20% variations in the percentage of sandstone and conglomeratic lithofacies over distances of 100-400 m. WX1 comprises calcareous mudstones in both the basin floor and up-dip Ilias delta. This is overlain by a coarser grained package, WX2, which thins and pinches out to the south in the G4 locality (Figure 2,3). WX2 comprises sandstone-rich and conglomeratic sheets and lenticular heterolithic packages in the basin floor, with highly variable conglomeratic and sandstone-rich scour-fills in the Ilias fan delta region. The overlying WX3 stratigraphy comprises sandstone- and conglomerate-rich broad, shallow, channel-fills interspersed with more lenticular but laterally extensive sandstone-rich heterolithics. WX3 is bound by its lower surface, Surface 3, which deeply incises within a 7 km^2 area of the Ilias fan delta foresets and bottomsets marks a major change in sedimentary facies from interbedded sandstone and mudstone foresets to conglomerate-rich foresets (Cullen et al., 2020). Near G4, Surface 3 comprises a surface separating underlying calcareous mudstones (WX1) and sandstone- and conglomerate-rich channelised lobe deposits (WX3 – Figure 3, 4, Cullen et al., 2020). Surface 4, the basal surface of WX4, marks a retrogradation of the Ilias fan delta, which is recognised by overlying back-stepping finer-grained (sandstone- and mudstone-rich) foresets, and corresponds to a downdip hiatus in coarse-grained siliciclastic supply to the deep-water (Figure 3, 4, Cullen et al., 2020). WX4 forms a regionally extensive mud-rich marlstone dominated unit with rare shelly fauna in the otherwise non-fossiliferous G4 core. WX4 is capped by Surface 5, marked by downlap of WX5 foresets onto WX4 foresets and bottomsets, reflecting renewed progradation of the Ilias fan delta (Cullen et al., 2020). At the G4 borehole, Surface 5 is overlain by conglomeratic debrites and sandstone sheets interbedded with mudstone horizons typical of WX5. The vertical change from WX4 to WX5 is laterally variable, appearing in G4 as ~90 cm thick debrite, but 500 m to the north as a gradual increase in the number and thickness of sandstone beds (Figure 3, 4). Surface 6 (base WX6) is marked by an erosion surface in the bottomset of the Ilias fan delta, and an increase in the proportion of conglomerates that thin and lap onto the foreset (Cullen et al., 2020). Near G4, Surface 6 is identified by an overlying and extensive coarse-grained, conglomeratic package that marks the onset of alternations of decametric-scale, laterally extensive packages of sandstone- and gravel-rich stratigraphy interbedded with mudstones of WX6 (Figure 3). In the Ilias fan delta region, WX5 and WX6 are exposed in the bottomsets, comprising laterally variable conglomeratic lenses, and elsewhere as sandstone-rich channel- and scour-fills. The base of WX7 is marked by a laterally extensive mass transport deposit of variable character that is overlain by sandstone sheets and mudstone intervals similar to WX5 and WX6 (Cullen et al., 2020).

In the region of the G4 borehole, three cliff faces (two orientated N-S and one north facing, NE-SW oriented cliff) produce a promontory near the village of Skoupéika (Figure 1-4, Cullen et al., 2020). Present day structural dip is 10 - 15° eastward for much of the deep-water stratigraphy in the northern part of these cliffs, rotating to 15 - 20° southeastward around the G4 borehole. This forms a broad SSE-NNW striking anticline, approximately 500 m wide, dissected by smaller-scale faults in the region around logs 1 and 2 (Figure 3, 4), which we interpret formed above a blind intra-basinal fault, Minor Fault 1 (Supplementary Information 3, Cullen et al., 2020). Stratigraphic thinning of WX2 and WX3 toward this blind fault tip (Figure 4) supports the presence of a minor bathymetric high generated by the blind fault during WX2 and WX3 deposition (Cullen et al., 2020). The southward thinning means WX2 is likely absent or highly condensed in the G4 core. Subtle northward thinning of WX5 (and WX3) between logs 3 and 5 may be a result of incipient growth of the Lykoporiá Fault and the inception of a bathymetric high to the north of the section (Cullen et al., 2020). Observations of intra-basinal structures <1 km to the footwall of, and co-planar with, the Lykoporiá Fault that affect younger stratigraphy (in WX7, WX8) support this interpretation (Figure 1, 2, Cullen et al., 2020).

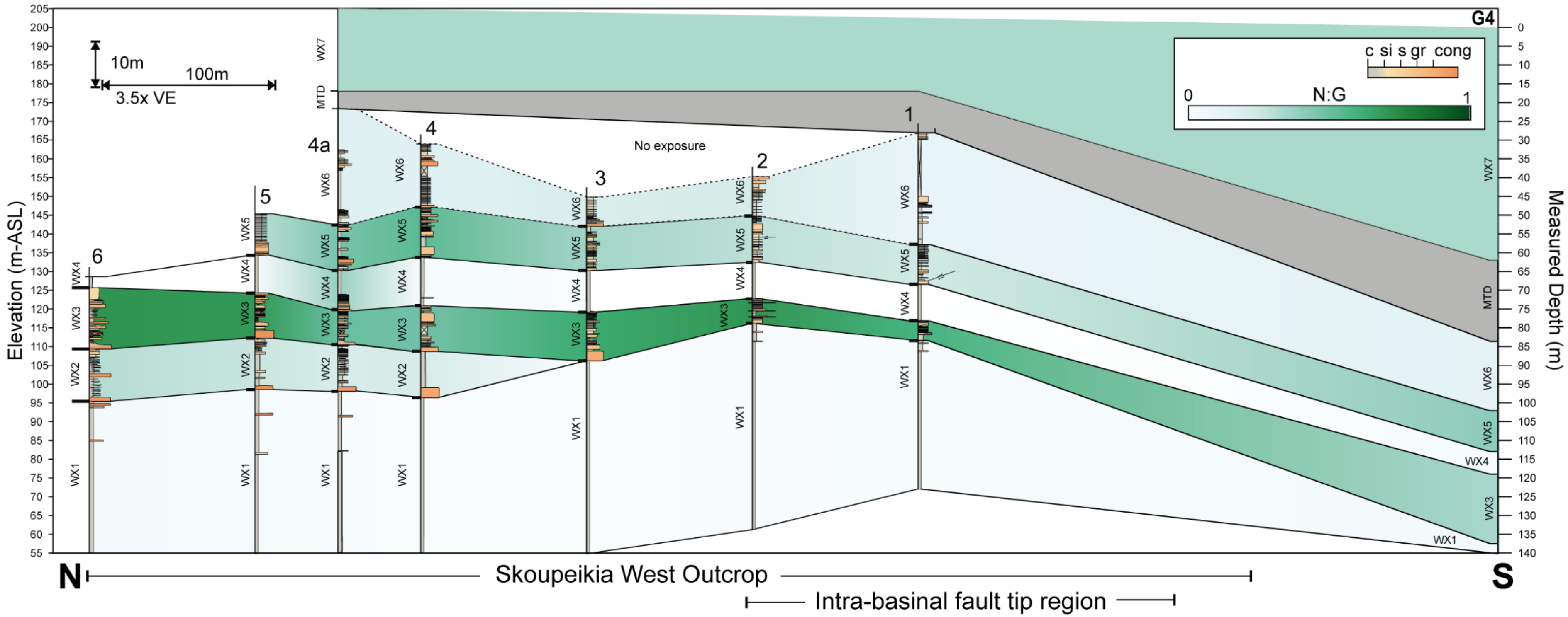

Figure 4: Correlation panel for the Skoupéika East outcrop into the G4 borehole with relative proportions of coarse-grained to fine-grained stratigraphy expressed as net:gross. Two main coarse-grained stratigraphic units (WX3 and WX5) are separated by mudstone rich WX4. MT and WX7 thicknesses are extrapolated from a digital log out of section by ~120 m downdip in line with 4a. The Skoupéika structure is complicated by an intra-basinal fault tip (probably related to Minor Fault 1), which generated a small anticline in the southern part of the cliffs and restricted the lateral extent of WX2. This produces the thinning relationships seen in WX3, WX4 and WX5, which show a northward and southward thinning from the central area (Log 4) where they are thickest.

5 Magnetic Chronostratigraphy

Biostratigraphy (low resolution palynology and macrofauna ranges) and tectonostratigraphy based on the topset elevations of laterally equivalent fan deltas and uplift rates for the southern margin of the Gulf of Corinth, place the Ilias fan delta system and downdip RDF stratigraphy to be ~1.5-0.7 Ma (Symeonidis et al., 1987; Muntzos, 1992; Armijo, 1996, Westaway, 2002; Malartre et al., 2004; Rohais et al., 2007a; Ford et al., 2007, 2013, 2016; Nixon et al., 2016, Gawthorpe et al., 2018). Syn-deformational calcite cements dated from the West Xylokastro Fault indicate activity on the West Xylokastro Fault at ~1 Ma (+/- 0.1 Ma) (Flotte et al., 2001; Causse et al., 2004), however such cements can be precipitated during various periods of the lifetime of a fault and do not constitute an upper boundary age condition. The youngest part of the West Xylokastro RDF is likely to coincide with the migration of activity from the West Xylokastro Fault to the Derveni and Lykoporiá Faults, which is estimated to have become the main active border fault at ~0.75 Ma (Bell et al., 2009; Nixon et al., 2016; Gawthorpe et al., 2018). Northward migration of fault activity may have been protracted, as timing of drainage reversals on the southern rift margin associated with this are known to range from 0.7-0.5 Ma (Ford et al., 2007; Gawthorpe et al., 2018; Fernández-Blanco et al., 2019, 2020; de Gelder et al., 2019).

Palaeomagnetic analyses from the G4 borehole and outcrop samples revealed six magnetozones within the West Xylokastro stratigraphy (Figure 3, 5). Two sections of normal (MAG1, MAG2) and reverse polarity (MAG0, MAG4) can be identified at the lower and upper parts of the stratigraphy, respectively (Figure 5). Within the ~1.5 – 0.5 Ma age range constrained by previous tectonostratigraphy and biostratigraphy, there are three > 20kyr periods of normal polarity; the Brunhes chron (0-773 kyr), the Jaramillo subchron (990 - 1001 to 1069 - 1071 kyr) and the Cobb Mountain subchron (1180 - 1215 kyr) (Figure 5). Shorter intervals of normal polarity (i.e. magnetic excursions) also exist and correspond to the Kamikatsura (867 kyr) and Santa Rosa (932 kyr) excursions.

An actively growing hanging wall depocenter north of the Lykoporiá Fault has been demonstrated from ~0.75 Ma (Nixon et al., 2016; de Gelder et al., 2019). This activity continued to the present day with uplift in the footwall of the Lykoporiá Fault acting to exhume the West Xylokastro RDF to its present-day position. The northward stratigraphic thinning within WX4 and WX5 across the northern part of the Skoupéika West outcrop panel (Figure 3, 4) is interpreted to reflect the onset of the earliest part of Lykoporiá Fault activity, where it formed a bounding topographic high to the West Xylokastro depositional system (Nixon et al., 2016; Gawthorpe et al., 2018; Cullen et al., 2020). As WX1 and WX2 was determined to be unaffected by the Lykoporiá Fault (Section 4), the MAG 1 normal polarity magnetozone should be older than ~0.75 Ma. The occurrence of a relatively thick reverse polarity magnetozone above MAG1 (i.e., MAG4) excludes the latter from being correlated with the Brunhes normal polarity chron.

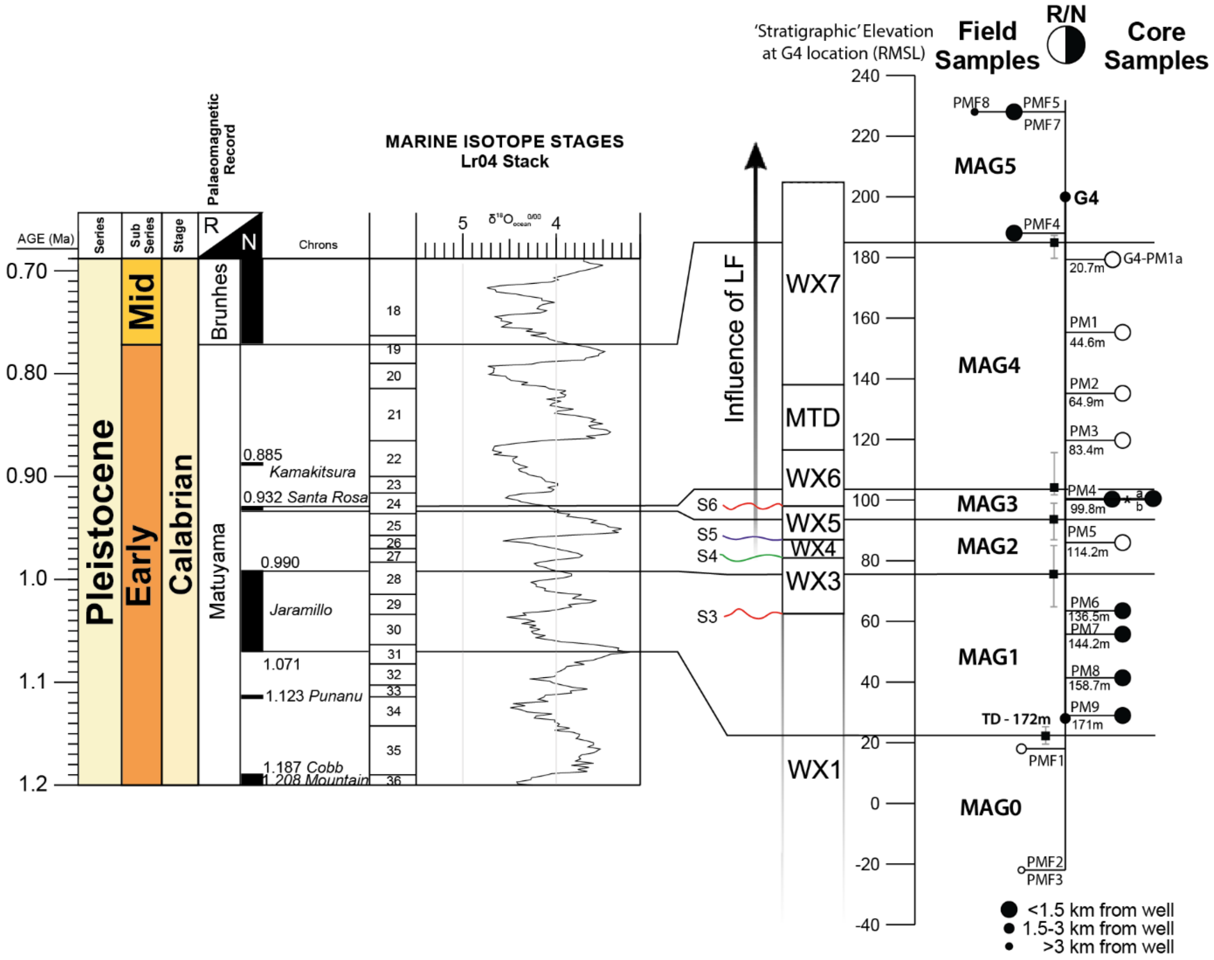

Figure 5: Palaeomagnetic ties of four reversals identified within the sampled stratigraphy to generate 6 magnetozones (MAG0-MAG5). Buffers in the placement of these reversals within the stratigraphy are shown as error bars in the sample locations on the right. Influence of Likoporia Fault (LF) determined from literature chronostratigraphic models and stratigraphic evidence in this study. * - Sample PM4 is confirmed by two additional samples G4-PM4a and G4-PM4b 30 cm and 15 cm above and below respectively.

In the absence of absolute stratigraphic ages (e.g. dated tephra), magnetostratigraphic logs can provide multiple, alternative age interpretations, as palaeomagnetic highlighted in Figure 6. The choice of the presented palaeomagnetic interpretation (MAG 1 = Jaramillo subchron) is in agreement with i) regional palaeogeography, ii) required exhumation/uplift rate, iii) rationality of sedimentation rates and/or variability, and iv) palaeomagnetic certainty (or variability thereof). In this instance, palaeomagnetic certainty relates to how likely the spot-sampling method would identify a given reversal, and/or how densely sampled a given magnetic chron is. With the exception of the Olduvai alternative, MAG1 Jaramillo, Cobb Mountain and Brunhes interpretations fit within the broad, possible age range (~1.8 Ma – ~0.6 Ma) for the RDF in the West Xylokastro Region (Ford et al., 2016; Gawthorpe et al., 2018; Figure 6). A "Brunhes Alternative" (Option 4 on Figure 6) can easily be ruled out as it would require the ~80m-thick MAG4 interval to have deposited within the ~10 kyr-long "Stage 17" excursion (Singer, 2014), hence providing an unrealistic sedimentation rate as high as 8 m/kyr or even more. Where MAG1 is tied to longer intra-Matuyama subchrons (i.e., Olduvai and Cobb Mountain) sedimentation rate variability would need to be extreme in order to fit palaeomagnetic data, and in cases outside typical values for similar settings of the Corinth Rift (0.2 m/kyr – 2.5 m/kyr as extremes; Ford et al., 2016; Sergiou et al., 2016; McNeil et al., 2019a). The estimated exhumation rate of the Likoporia Fault footwall to put the RDF at its present day position required for the oldest (Olduvai) alternative (~0.4 mm/yr) is substantially slower than that established for this region of the southern coastline (1.3-1.5 mm/yr - Armijo et al., 1996; Taylor et al., 2011; Ford et al., 2014, 2016; Rohais & Moretti, 2016; de Gelder et al., 2019). Past uplift rates may have been slower during the early life of the Lykoporiá Fault so this criterion alone is uncertain. However, if this were the case, such an uplift rate would place beach terrace deposits that lie unconformably on the RDF as significantly older (~750 ka) than elevation equivalent beach terraces to the east with confirmed U/Th dating (maximum 600 ka, Armijo et al., 1996). A 5th alternative is of a case where the stratigraphy stretches from the Olduvai subchron (1.8-~2 Ma) to the Brunhes Chron, with MAG3 tying to either the Jaramillo or Cobb Mountain subchron (Figure 6). In these cases, the conditions for regional palaeogeography, uplift rate and magnetic certainty are met. However, such a situation requires extremely low sediment accumulation rates of 0.02 to 0.03 m/kyr which are very unlikely given the relatively proximal location, and the grainsizes and lithofacies present. In addition, such a model would struggle to reconcile the existence of ~100 m of deltaic stratigraphy beneath WX1 exposed at the Ilias delta and poorly exposed 30 m sub-WX1 stratigraphy in the basin, which only began its growth at ~1.8 Ma (Gawthorpe et al., 2018). As a result, the chosen interpretation relies on MAG1 tying to the Jaramillo subchron, which yields sediment accumulation and uplift rates, and palaeogeographies, which agree with those established in the Corinth Rift, and has a reasonable palaeomagnetic certainty. This interpretation is further supported by the likely correlation of the short MAG3 normal polarity interval with the Santa Rosa excursion (Figure 5). The MAG3 normal polarity magnetozone is confirmed by two additional closely spaced samples (G4-PM4a and G4-PM4b), due to the weaker response of sample PM4 demonstrating a normal polarity over a 45 cm section (Supplementary Information 1 and 2).

Figure 6 (next page): Summary chart (A) for the four possible alternative palaeomagnetic interpretations for the West Xylokastro RDF stratigraphy in this thesis. B) Sediment accumulation rates for magnetozones (MAG0-5) for the four possible scenarios. Red text indicates sediment accumulation rates (m/kyr) which are far outside previously documented ranges for similar settings or are of extreme variability. C) Summary of interpretation choice based on agreement with well-established regional palaeogeographies, required uplift rates, sedimentation rates, and the ability for the palaeomagnetic survey in this study to detect the required variations. Sedimentation rates for magnetozones 0 and 5 are less constrained than MAG1 – MAG4 due to no 'bounding' reversal at the base and top of stratigraphy and so are estimated as maximums, to the nearest adjacent reversal or extrapolation of the maximum preserved thickness. Geomagnetic Instability Time Scale (GITS) palaeomagnetic record from Singer et al. (2014) and Ogg (2020). Duration for Santa Rosa (case 1) taken from Yang et al. (2004). Duration for Punaruu from Channell (2017). Minor Brunhes excursion durations deemed as ~1kyr from Singer (2014), likely not truly detectable in this survey. Sample PM4 (MAG 3) is confirmed by two additional samples G4-PM4a and G4-PM4b 30 cm and 15 cm above and below respectively for clarity on the scale of the figure this is reduced to a single dot.

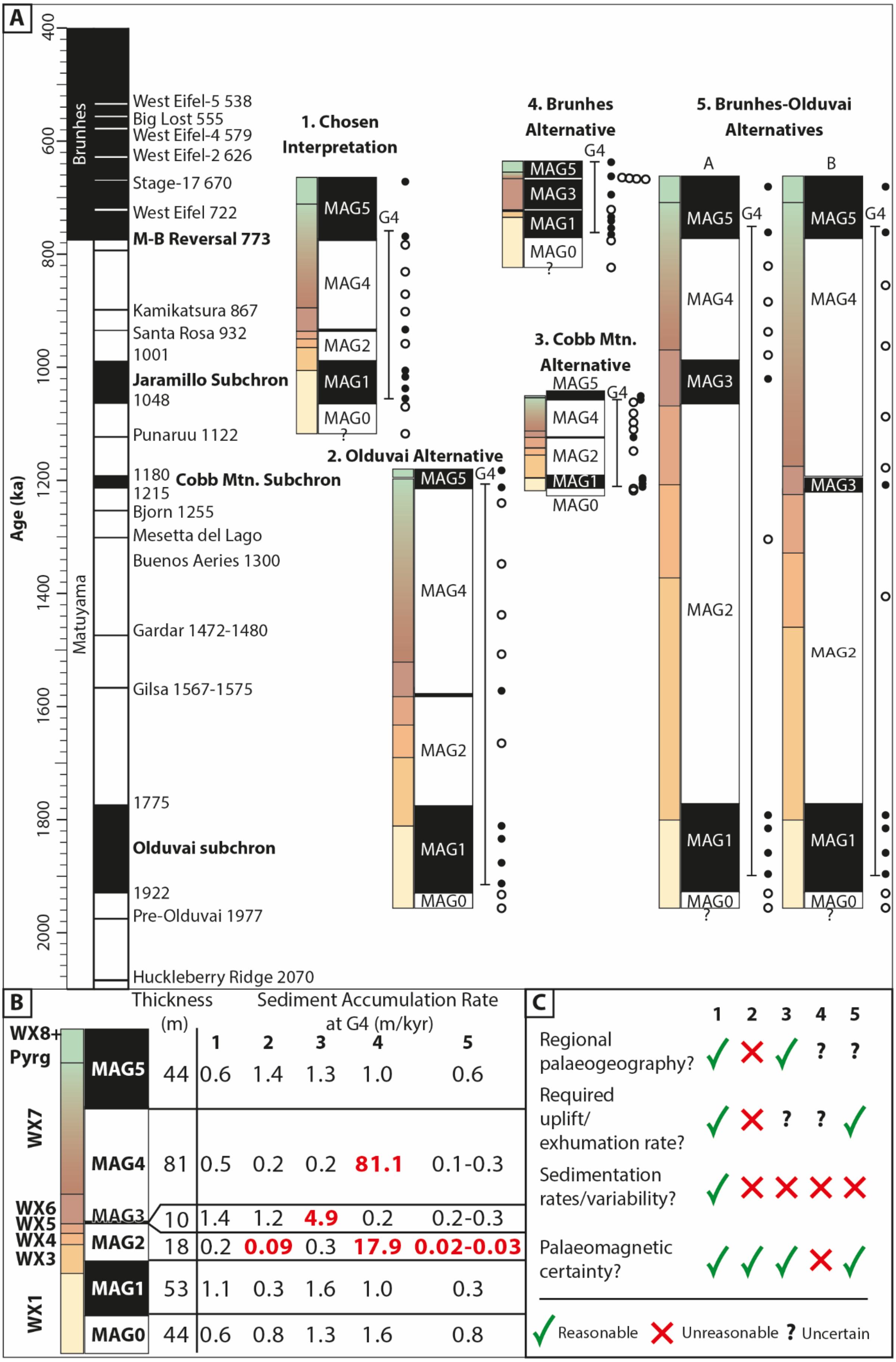

	Thickness (m)	Sediment Accumulation Rate at G4 (m/kyr) 1	2	3	4	5
MAG5	44	0.6	1.4	1.3	1.0	0.6
MAG4	81	0.5	0.2	0.2	**81.1**	0.1-0.3
MAG3	10	1.4	1.2	**4.9**	0.2	0.2-0.3
MAG2	18	0.2	**0.09**	0.3	**17.9**	**0.02-0.03**
MAG1	53	1.1	0.3	1.6	1.0	0.3
MAG0	44	0.6	0.8	1.3	1.6	0.8

	1	2	3	4	5
Regional palaeogeography?	✓	✗	✓	?	?
Required uplift/ exhumation rate?	✓	✗	?	?	✓
Sedimentation rates/variability?	✓	✗	✗	✗	✗
Palaeomagnetic certainty?	✓	✓	✓	✗	✓

✓ Reasonable ✗ Unreasonable ? Uncertain

Two hundred metres of younger RDF stratigraphy is preserved as the Upper WX (Cullen et al., 2020). Extrapolating the preferred uppermost sediment accumulation rate estimated from the palaeomagnetic ties for MAG 4 gives an age of ~0.6 Ma for the top of the preserved West Xylokastro RDF stratigraphy in the study area. Internal to these upper and lower boundaries, the positioning of stratigraphic units needs to account for condensed sections. Unit WX2 is absent, or condensed, at the base of WX3 as a composite of WX2 and Surface 3 within the G4 borehole stratigraphy (Figure 3). Using the nearby G4 borehole sediment accumulation rate from analogous MAG1 (0.65 m/kyr) or MAG2 (0.42 m/kyr), and thickness of WX2 at its thickest point nearby (~15 m in Log 6 in Figure 3), WX2 is interpreted to correspond to a ~23 kyr–36 kyr duration. The preferred duration is the shorter model, given the greater similarity of stratigraphy within MAG1 to that of MAG2, which contains a basin wide mudstone interval separating coarse-grained scour-fill prone stratigraphy, rather than the alternations between mudstones and laterally extensive conglomeratic debrites and mudstones within MAG1.

The chronostratigraphic placement of the West Xylokastro Fault Block stratigraphy places it equivalent to the lower offshore unit penetrated at IODP 381 Site M0078 (Unit 1 - Nixon et al., 2016; Unit 2 - McNeil et al., 2019a-f) and provides one of the first demonstrable chronostratigraphic ties between the onshore and offshore stratigraphy in the Gulf of Corinth. Chronostratigraphy established through the palaeomagnetic record also allows context for the likely frequency recorded by palynological sampling, which averages 1 sample per 20kyr, although this rate does show minor deviations to maintain good sample quality. This means the palaeoenvironmental record will not accurately characterise higher-frequency variability (~10^3 kyr).

6 Palynology

6.1 Palynofacies analysis

All palynological samples plot within the proximal, terrestrially-influenced part of a palynofacies ternary plot (Figure 7, *sensu* Tyson, 1996, Zobaa et al., 2015). An enlargement of the upper 20% of the ternary plot (Figure 7b) highlights that very minor marine/brackish influences are typically within mudstone-rich units (WX4 and WX1) or more heterolithic units (WX5/6). These are expressed as minor (<5%) occurrences of AOM and marine algae (Supplementary Information 4), dinoflagellates, and a coincident reduction of freshwater algae and/or terrestrial matter. Occurrences of marine algae are very low (single grains) and commonly have a highly degraded appearance. Figure 8 provides further detail on the types of organic matter preserved and highlights consistently high cuticle/unstructured phytoclasts and woody/equant/bladed debris comprising 40-70% of the organic matter. There is no observable cyclicity in this organic matter type or distribution, and variability is generally pulsed (rather than cyclical waxing or waning variability). Pulses of freshwater algae (*Botryococcus)* are noted at the onset of WX6 and are at their lowest during mudstone dominated WX1 and WX4, and sandstone-rich WX5. Within WX7, very high proportions of equant debris and degraded wood are recorded with far less cuticle than in lower parts of the succession.

The dominance of terrestrial palynomorphs, and the lack of strong marine influence indicators, agrees with previous studies that interpret the first phase of the Late Pleistocene Gulf of Corinth as a largely isolated freshwater to brackish body: “Lake Corinth” (Rohais et al., 2008, Gawthorpe et al., 2018, McNeil et al., 2019a, f). In WX4 and WX5, possible marine indicators such as AOM and NTP remain below the 2% of the SOM at their highest level in the stratigraphy. NTP (e.g. Marine Algae, Acritarchs and Zoomorphs), when present, are found in very low numbers, and detailed identification was not possible. As a result, minor presences of NTP cannot be considered as indicative of marine conditions given the overwhelmingly freshwater signature even where they are present. However, we cannot exclude that this may be indicative of some presence of partly mixed or weakly brackish conditions due to the level of poor preservation of acritarchs present. Given the co-occurrence with more strongly represented *Spiniferites cruciformis* (Figure 8), pulses of NTP may be related to minor salinity variations due to increased freshwater/terrigenous influx (Kouli et al., 2001; Mudie et al., 2017) comprising rarer freshwater acritarchs, however this cannot be confirmed. The intra-WX7 switch to equant debris/degraded wood dominated organic assemblages is interpreted as results of depositional palynofacies variation (McArthur et al., 2016a, b) corresponding with change from lobate/weakly confined deposits to more channelised stratigraphy within WX7 (Cullen et al., 2020).

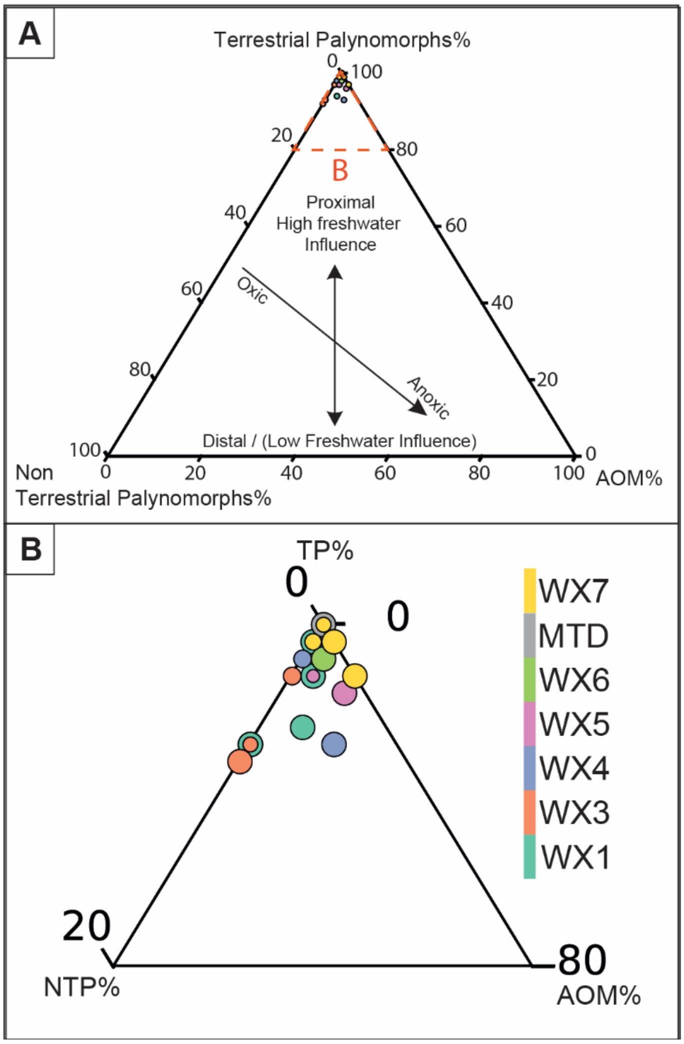

Figure 7: A) Environmental importance of relative percentages on ternary palynology plots of percentages of TP (Terrestrial Palynomorphs), NTP (Non-Terrestrial or 'marine' Palynomorphs) and AOM (Amorphous Organic Matter). Modified after Zobaa et al. (2015) and Tyson (1996) in a Full scaled ternary plot for G4 palynology samples highlighting strong freshwater influence in all samples. B) Blow out of upper 20% triangle highlighting minor deviations to weak marine (or saline) influences (<5%).

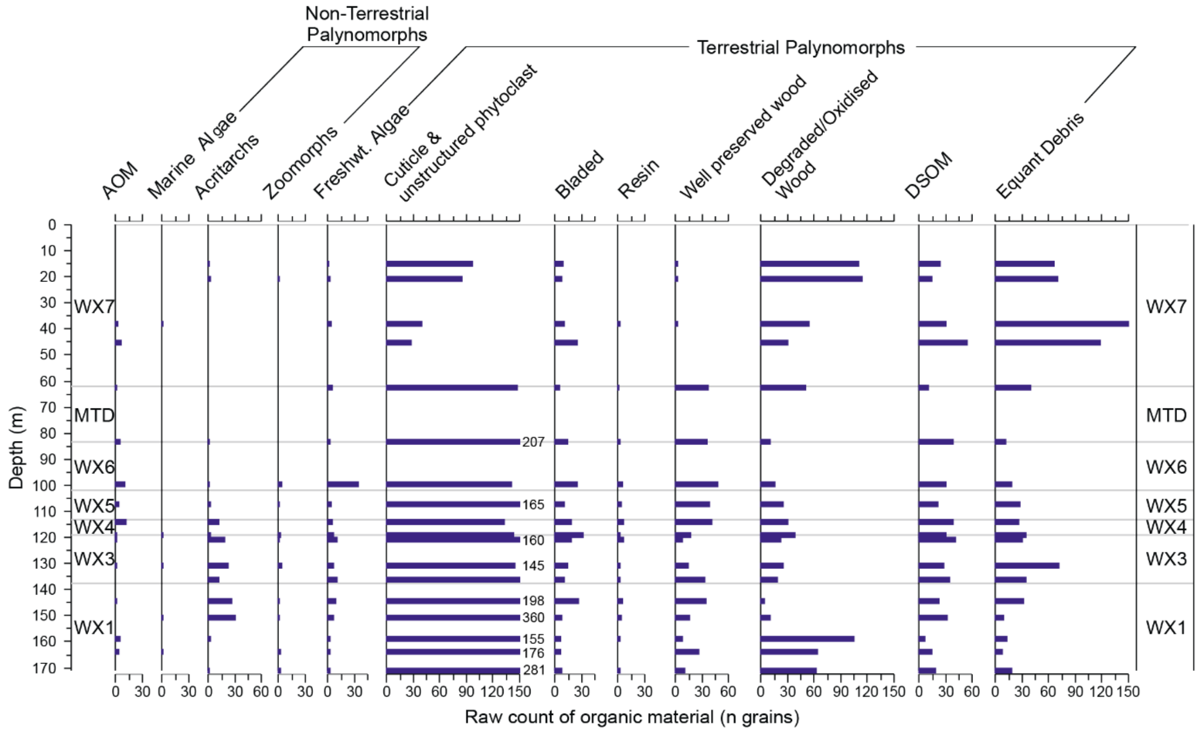

Figure 8: Summary stratigraphic plot of raw count data for sedimentary organic matter (excluding pollen, spores and dinoflagellates). X-axes are absolute numbers of particles, with numbers provided where the x-axis is exceeded.

6.2 Dinoflagellates and non-pollen palynomorphs (NPP)

The maximum number of co-existent dinoflagellate taxa is 11, with most samples typically showing 3 – 5 taxa (Figure 9). *Spiniferites* spp. and *Spiniferites cruciformis* exhibit the highest abundances as peaks within WX1, near the top of WX4, within WX5, and near the base of WX6. Other dinoflagellate cyst taxa occurrences also increase in samples with high *Spiniferites* spp. counts but are typically lower in abundance. During WX5 and WX6, high abundance of *Spiniferites* spp. is coincident with increases in freshwater algae (Figure 7, Supplementary Information 4). In contrast, during WX3 when *Spiniferites* spp. counts are substantially lower, there is an increased presence *of Impagdinium, Gymnodinium* and *Ataxiodinium choane* cysts. Acritarchs are rare in most samples, and where present are poorly preserved, meaning their genera cannot be identified.

The variable presence and limited dinoflagellate diversity reflected by the relatively low number of taxa suggests that dinoflagellate populations may have been strained (Mudie et al., 2001). High concentrations of *S. cruciformis* and lower dinoflagellate diversity suggest the area was isolated from the Mediterranean Sea during this interval. Such almost monospecific dinoflagellate cyst assemblages are found in the lowest salinity, isolated intervals in the late Pleistocene Gulf of Corinth (McNeil et al., 2019a-f, Fatourou et al., 2021) in contrast to more diverse assemblages during marine connections (Collier et al., 2000; McNeil et al., 2019a-f). The co-presence of *S. cruciformis* and *Spiniferites* spp. accompanied with relative increases in freshwater algae (e.g. in WX5 in Figure 8), is in agreement with the recognised ability of *S. cruciformis* to withstand a variety of salinity conditions (Kouli et al., 2001; Mertens et al., 2012a; Mudie et al., 2001; McNeill et al., 2019e) and its characterisation as a ‘pioneer’ taxa in strained or variable salinity environments such as the Black Sea corridor (Mudie et al., 2001; 2010; 2017). Mudie et al. (2010) highlight that nutrient supply to the water-column rather than absolute lake-level and marine-connectivity controls *Spiniferites* spp. populations in lacustrine or ephemerally connected water bodies. As a result, variability in diversity and/or presence of dinoflagellate populations may be linked to minor variations in salinity resultant from increased fresh-water influx to a given basin. Ultimately, the dinoflagellate and other non-pollen palynomorph signature is consistent with the entire G4 stratigraphy being deposited under largely lacustrine conditions, in agreement with the lower unit of IODP boreholes M0078 and M0079 in McNeil et al. (2019a-f). The very minor occurrences of degraded marine algae may be reworked organic material from basement rocks, or could possibly reflect the distal effects from minor, weak marine incursions from the eastern end of the rift at the Corinth Isthmus (Rohais et al., 2007b, Gawthorpe et al., 2018).

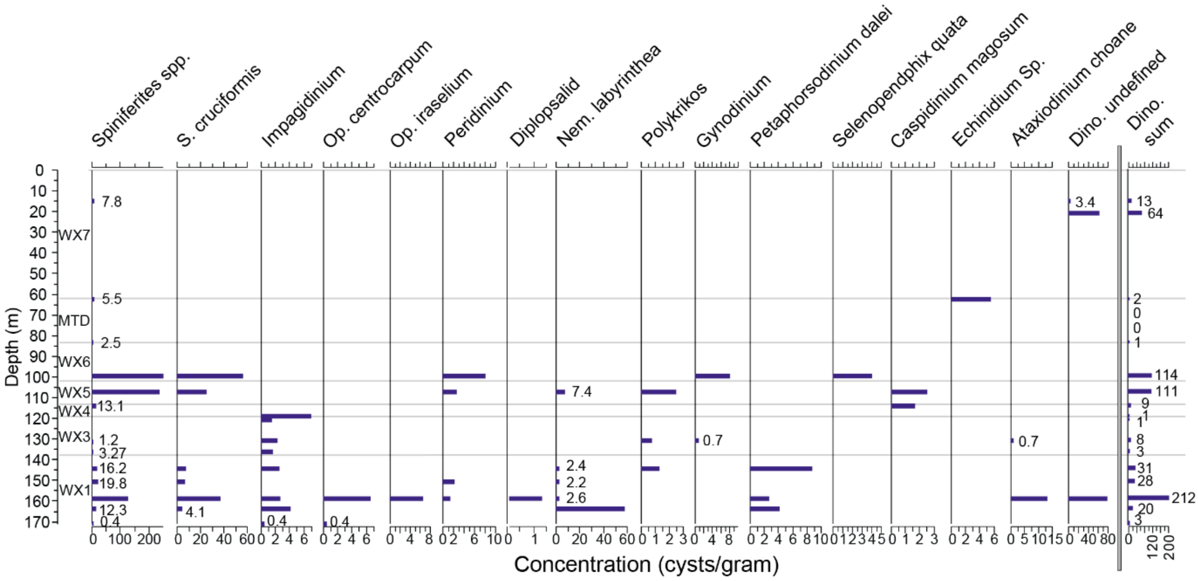

Figure 9: Stratigraphic summary for dinoflagellate cysts presented as concentrations (cysts/g). Small values/low occurrences are labelled along with a ‘Dino Sum’ (total number of dinoflagellate cysts in each sample) curve.

6.3 Pollen assemblages

Figure 10 presents the pollen concentration data from the G4 borehole (Supplementary information 4). *Pinus* and Pinaceae are generally the most common taxa, except for minor periods when grasses (Poaceae, Cyperaceae) dominate the assemblages outside of which they are typically the second most abundant taxa. The next most common taxa are Poaceae, Cyperaceae and subordinate Asteraceae, Cupressaceae/Taxodiaceae and *Plantago* sp. (Figure 10c). As with most Pleistocene pollen records, substantial variability exists in the abundance of arboreal pollen (Tzedakis et al., 2006; Joannin et al., 2007a,b; Okuda et al., 2008; Sadori et al., 2016). The assemblage is similar to most Pleistocene Mediterranean assemblages, although *Artemisia* is notably absent. Unlike other Mediterranean

Pleistocene pollen records, *Quercus* makes up a comparatively minor component of arboreal pollen in the G4 stratigraphy (Tzedakis et al., 2006; Joannin et al., 2007a, b; Okuda et al., 2008; Sadori et al., 2016). Mediterranean elements (a taxon group defined in Figure 10 based on Joannin et al., 2007) are also very rare in the G4 record, similar to their scarcity in IODP 381 Corinth Rift palynological observations (McNeil et al., 2019a,b,e,f). Steppic elements, such as Chenopodiaceae or *Ephedra*, are present but rare, with aquatic elements (Potamogetonaceae, Sparganiaceae and *Nymphea alba*) even rarer. Other herbaceous elements comprise flowering plants typical of, although not specific to, flora assemblages in Quaternary Mediterranean studies (e.g. Joannin et al., 2007a,b). Most commonly in this study these comprise Asteraceae, Caryophyllaceae, Saxifragaceae, Rosacae, Dipsaceae, Malvaceae and the relict taxon *T. sibiricum*.

Biome affinities (Figure 10b) are typical of Quaternary Mediterranean flora assemblages in the large altitudinal range (0 – 1500 m) which surrounds the modern Gulf of Corinth (Marinova et al., 2018). The strongest biome affinities are towards with Graminoids with Forbs (GRAM), followed by cold and cool evergreen needleleaf forest (CENF and COOL), temperate deciduous malachophyll (TEDE), cool mixed evergreeen needleleaf and deciduous broadleaf forest (CMIX), and warm-temperate evergreen needleleaf and sclerophyll broadleaf forest (WTEF). Non-forested biomes are strongly represented by graminoid grasslands (GRAM) and a more minor and variable xeric shrubland component (XSHB).

Figure 10: (Next 2 pages) A) Detailed concentration (thousands of grains per gram) diagram of all pollen taxa identified, showing the constituent taxa of groupings. Pollen sum (total counts) are also provided. B) Upper: Pollen groupings plot in percentages along with total pollen sum and Lower: Biomization summary highlighting the G4 data with an environmental key and conceptual after Marinova et al. (2018) highlighting the general temperature and precipitation conditions the biomes exist under. Boxes surrounding points on the biome affinity plot highlight the 5 strongest affinities for a given sample, where more than 5 are highlighted this reflects where biomes have equal affinities. The modified Marinova et al. (2018) conceptual model is reproduced with permission from John Wiley & Sons (License No. 5072700384261).

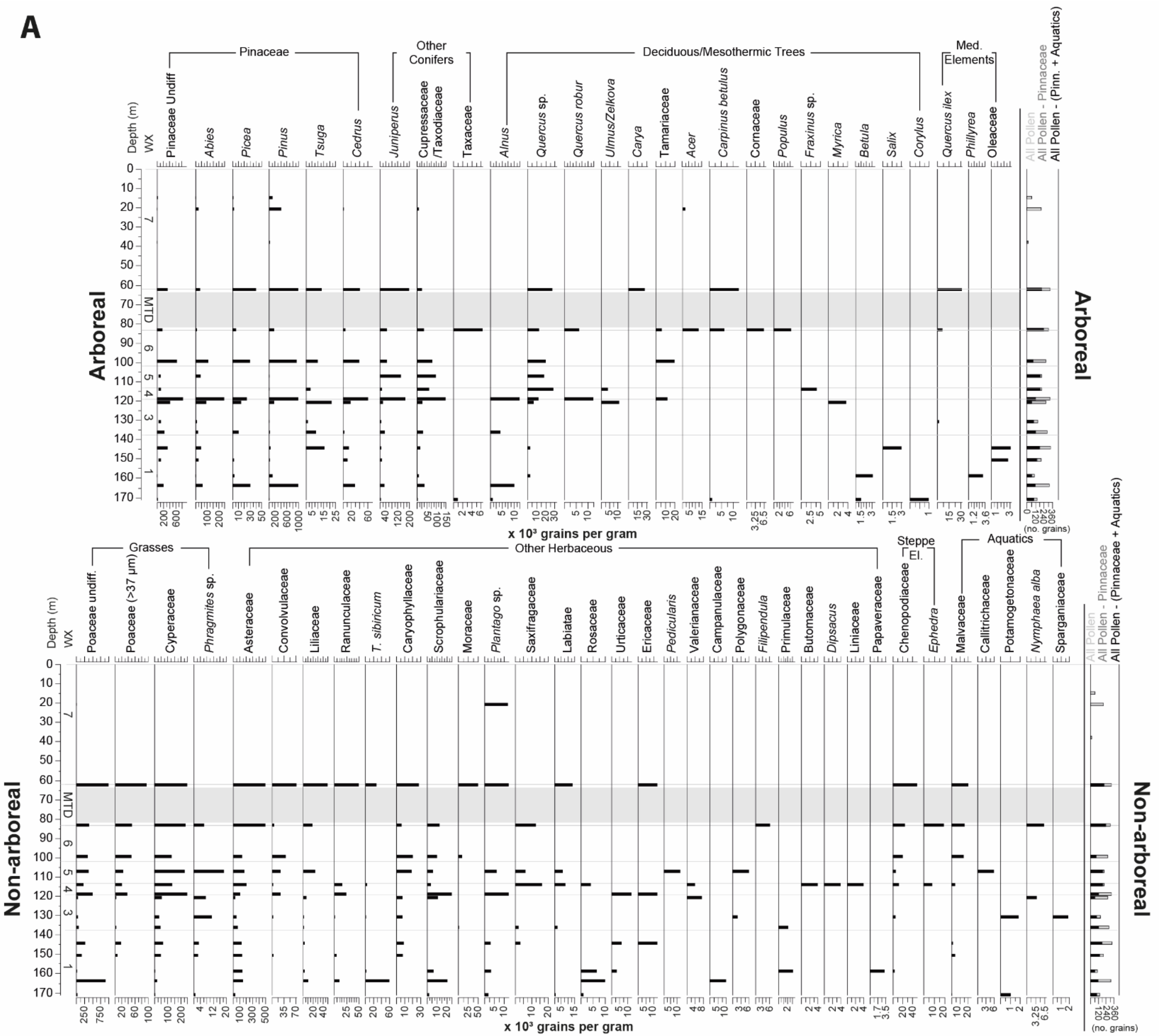A
Arboreal
Non-arboreal
Depth (m)
WX
MTD
Pinaceae
Other Conifers
Deciduous/Mesothermic Trees
Med. Elements
Pinaceae Undiff
Abies
Picea
Pinus
Tsuga
Cedrus
Juniperus
Cupressaceae /Taxodiaceae
Taxaceae
Alnus
Quercus sp.
Quercus robur
Ulmus/Zelkova
Carya
Tamariaceae
Acer
Carpinus betulus
Cornaceae
Populus
Fraxinus sp.
Myrica
Betula
Salix
Corylus
Quercus ilex
Phillyrea
Oleaceae
All Pollen
All Pollen - Pinnaceae
All Pollen - (Pinn. + Aquatics)
(no. grains)
x 10³ grains per gram
Grasses
Other Herbaceous
Steppe El.
Aquatics
Poaceae undiff.
Poaceae (>37 µm)
Cyperaceae
Phragmites sp.
Asteraceae
Convolvulaceae
Liliaceae
Ranunculaceae
T. sibiricum
Caryophyllaceae
Scrophulariaceae
Moraceae
Plantago sp.
Saxifragaceae
Labiatae
Rosaceae
Urticaceae
Ericaceae
Pedicularis
Valerianaceae
Campanulaceae
Polygonaceae
Filipendula
Primulaceae
Butomaceae
Dipsacus
Liniaceae
Papaveraceae
Chenopodiaceae
Ephedra
Malvaceae
Callitrichaceae
Potamogetonaceae
Nymphaea alba
Sparganiaceae
All Pollen - (Pinnaceae + Aquatics)
0
10
20
30
40
50
60
70
80
90
100
110
120
130
140
150
160
170
7
6
5
4
3
1

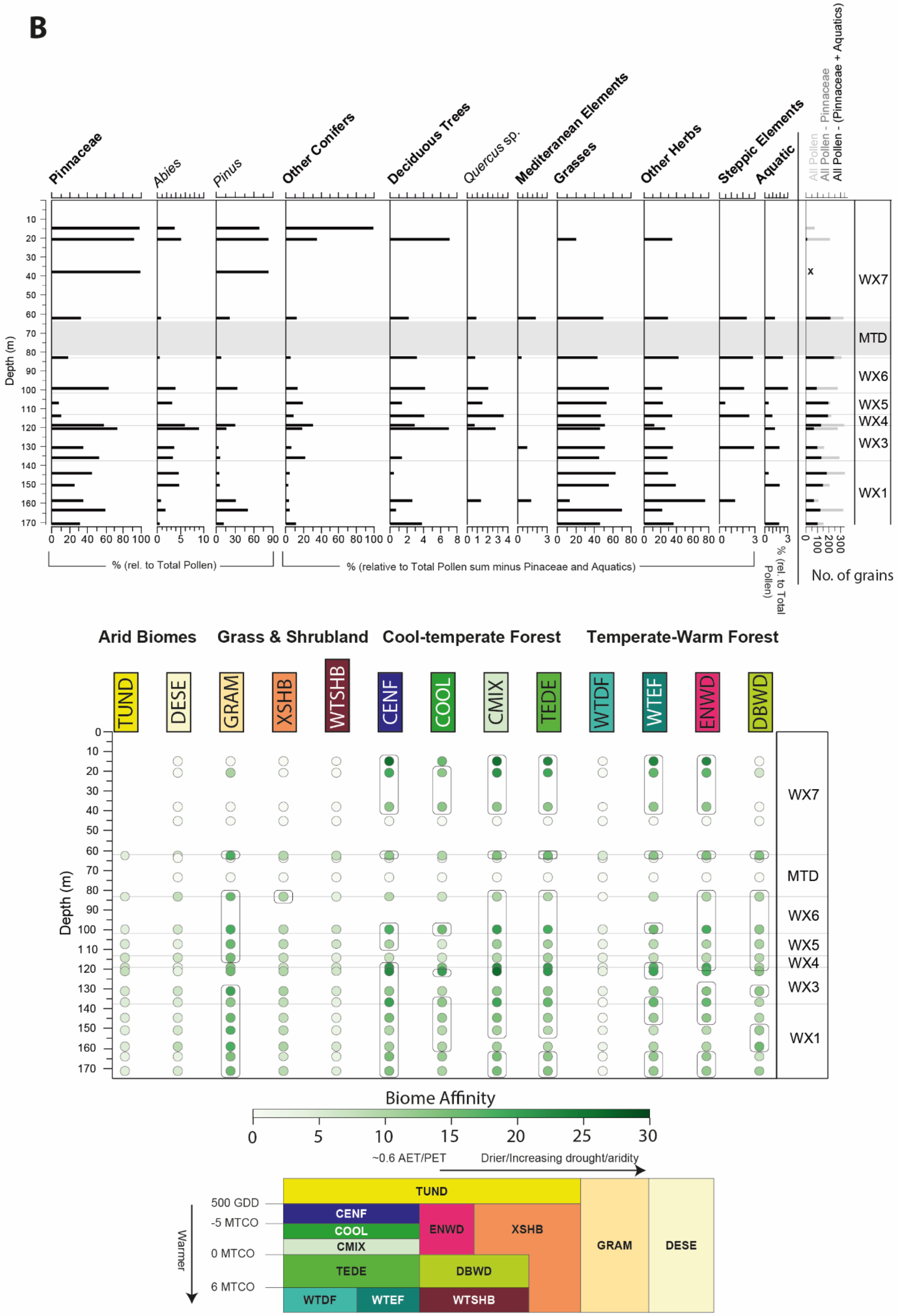
B
Pinnaceae
Abies
Pinus
Other Conifers
Deciduous Trees
Quercus sp.
Mediteranean Elements
Grasses
Other Herbs
Steppic Elements
Aquatic
All Pollen
All Pollen - Pinnaceae
All Pollen - (Pinnaceae + Aquatics)
Depth (m)
% (rel. to Total Pollen)
% (relative to Total Pollen sum minus Pinaceae and Aquatics)
% (rel. to Total Pollen)
No. of grains
WX7
MTD
WX6
WX5
WX4
WX3
WX1
Arid Biomes
Grass & Shrubland
Cool-temperate Forest
Temperate-Warm Forest
TUND
DESE
GRAM
XSHB
WTSHB
CENF
COOL
CMIX
TEDE
WTDF
WTEF
ENWD
DBWD
Biome Affinity
0
5
10
15
20
25
30
~0.6 AET/PET
Drier/Increasing drought/aridity
500 GDD
-5 MTCO
0 MTCO
6 MTCO
Warmer

WX1 is largely characterised by high proportions of non-arboreal pollen, grasses and a diverse array of other herbaceous taxa. Arboreal pollen abundance varies between ~<250k grains/gram to more than 1600 grains/gram with two distinct peaks. Arboreal pollen is dominated by *Pinus*, and more commonly Pinaceae Undiff. and Abies towards the uppermost part with deciduous trees being generally rare. Non-arboreal pollen mostly comprises Poaceae and other herbs (most commonly Asteraceae and *T.sibiricum* although the non-arboreal taxa present are diverse and variable). Steppic elements and Mediterranean elements are generally absent, with the exception of some rare representation in the middle and upper part of the unit. The middle portion of the unit shows less coniferous arboreal pollen (most dramatically in *Pinus*) but the strongest presence of mesothermic trees (*Betula* and *Quercus*) and scleroyphyllous (scrub) forms of herbaceous plants (e.g. Scrophulariaceae, and steppic elements). As a result, there is a weakened affinity towards temperate forested biomes in the middle part of WX1, with biome affinities stronger towards graminoid grassland and xeric shrubland (Figure 10b). In the upper part of WX1, grassland is dominant with a minor component of coniferous trees (especially *Abies, Picea, Juniperus* and other Cupressaceae). The uppermost part of WX1 has approximately equal affinities towards graminoid grassland (GRAM), cool evergreen needle leaf forest (CENF) and cool mixed evergreen needleleaf and deciduous broadleaf forest (CMIX) and evergreen needleleaf woodland (ENWD) suggesting a temperate-cool climate. Whilst the strong affinity towards forest throughout the unit indicates sufficient precipitation, increases in affinities within the middle of the unit to xeric biomes and sclerophyllous vegetation suggest potential periods of lower precipitation.

Overall, WX3 shows comparably lower arboreal pollen percentages and a dominance of non-arboreal pollen, rich in grasses (Cyperaceae and *Phragmites sp.*) and other herbs (Asteraceae, Caryophyllacae). The arboreal pollen assemblage is dominated by conifers with mountainous/cold-tolerant taxa, such as *Abies* and more minor *Tsuga* (Figure 10). The conglomerate- and sandstone-rich lower-to-middle part of WX3 also shows peaks in steppic (Chenopodiaceae) and aquatic elements. Following this, there is an expansion of forest cover through the upper part of WX3, especially in deciduous trees (mainly *Quercus and Ulmus)* through the unit from <2% at its base to ~8% in the upper part of WX3. As a result, samples immediately prior to WX4 show strong affinities only towards forested biomes, some of which require warm or temperate climates (Figure 10b - e.g. WTEF). The lower part of WX3 is therefore interpreted to represent a mix of steppe/grassland vegetation initially with more minor forest cover typical of a colder, likely wetter climate associated with Pleistocene glacials in the Mediterranean (Collier et al., 2000; Tzedakis et al., 2006; Joannin et al., 2007a, b). This is followed by a warming in the transition from WX3 to WX4 which is accompanied by a decrease of steppic and Mediterranean elements, suggesting an increase in precipitation supported by weakening affinities to grassland (GRAM), xerophytic shrubland (XSHB) and any desertification (DESE) indications.

Mudstone-dominated WX4 comprises a ~8 m section showing substantial differences between a mixed-arboreal-dominated lower part and a non-arboreal-dominated upper part with the arboreal percentage is dominated by deciduous trees (*Quercus* sp., *Ulmus* and *Fraxinus* sp.). The lower part of WX4 is dominated by arboreal pollen, which is largely conifer-dominated. Comparatively, the upper part of WX4 records a substantial decrease in conifer pollen, as part of an overall 60% reduction in arboreal pollen from the onset of WX4 to the base of WX5. However, the mesothermic/deciduous proportion comprising *Quercus* and *Alnus* remains low in the upper and lower part of WX4 (~3-5%). This marks a shift in the forest biome affinities from cool or cold-forest (e.g. CENF, COOL), with graminoid grassland (GRAM) in the lower part of WX4 towards more temperate mixed forest biomes (TEDE, CMIX, ENWD, DBWD) through to WX5 with maintained strong affinities towards graminoid grassland (GRAM). More subtle changes also exist, such as increased diversity of other herbaceous elements, with 10 co-existent taxa, but still dominated by Asteraceae. Whilst desert/xeric biomes (mainly represented by steppic elements) remain relatively low, these biomes approximately double their affinity from the onset of WX4 to the onset of WX5. The low values of DESE and XSHB likely reflect the lower pollen dispersal potential compared to Pinaceae and other arboreal taxa, but nevertheless show an increase during this time. The combination of the i) overall reduction in arboreal pollen, but maintenance of deciduous trees, ii) increase in xeric and desertification indicators, and iii) an absence of cold or humidity-demanding taxa such as *Abies*, is interpreted to reflected continued warming and drying, to a climate too warm, or too dry, to sustain widespread temperate or cool coniferous forest. This assemblage is maintained through much of the heterolithic but sandstone-rich WX5, with an absence of *Pinus* and very low counts of other Pinaceae. The uppermost 4-5 m in WX5 records a change, with increased coniferous arboreal pollen, and decreased mesothermic arboreal elements (*Quercus* sp.) indicative of return to a cooler, temperate or wetter climate, with a notable switch to strong affinities to CENF and COOL forest in addition to TEDE, CMIX and WTEF.

WX6 comprises approximately equal proportions of arboreal and non-arboreal pollen in the lowest sample and is more dominated by non-arboreal pollen at its top. The basal part of WX6 contains a diverse array of non-aboreal pollen and some of the largest abundances of aquatic and steppic elements through the G4 record. Initially this is accompanied by a minor, mixed arboreal proportion comprising *Quercus* sp., Tamaricaceae mesothermic/deciduous trees, and humidity demanding Pinaceae taxa, such as *Abies*. The upper part of the unit shows less conifers and grasses but similar, overall deciduous tree percentage (~5%), and is dominated by grasses and steppic and aquatic elements. Biome affinities to frost-intolerant or temperate biomes (e.g. WTEF) are low while affinities to grassland and xeric shrubland biomes appear increased. This is ultimately interpreted as continuation of the cooling at the end of WX5, to a colder and less-forested landscape. The MTD overlying WX6 is followed by more sparsely sampled and occasionally barren stratigraphy (Figure 10, Supplementary Information 4). Given the poor sample preservation within and above the MTD, we do not propose a confident climatic interpretation for WX7 stratigraphy on the basis of the G4 pollen record.

7 Discussion

7.1 Palaeoenvironmental evolution and sediment supply synthesis

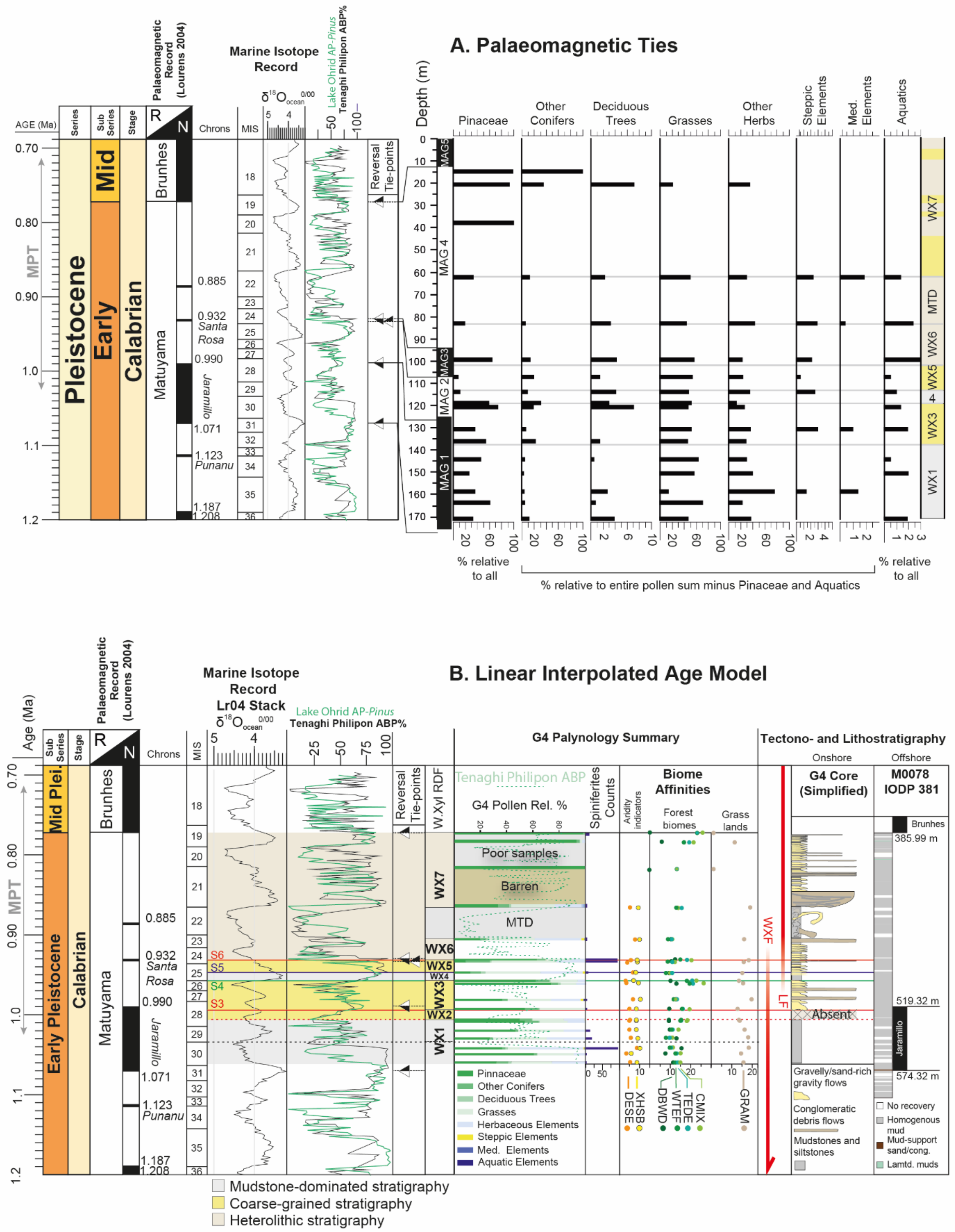

Figure 11: A) Summary of palaeomagnetically tied intervals of the G4 palynological record. B) Age model for G4 stratigraphy using linear time-depth relationship/sedimentation rate within magnetozones. Palaeomagnetic tie-points from the G4 stratigraphy are highlighted with triangles where black represents normal polarity, and reversed

represented by white. A subset of biome affinities are also shown; DESE - Desert, XHSB - Xerophytic Shrub, GRAM - Graminoids with Forbs, DBWB - Deciduous broadleaf woodland, WTEF - Warm-temperate evergreen needleleaf and sclerophyll broadleaf forest, TEDE, Temperate deciduous malcophyll broadleaf forest and CMIX - Cool mixed evergreen needleaf and deciduous broadleaf forest. Onshore bed thicknesses are not representative of actual bed thicknesses. Equivalent offshore stratigraphy is from IODP Hole M0078 after McNeil et al. 2019f (N.B Colour schemes are altered from McNeil et al., 2019a-f for simpler comparison here). Tenaghi Philippon Arboreal Pollen Percentage is retrieved from the updated age model of Wagner et al. (2018), Lake Ohrid Arboreal Pollen (minus Pinus) record from Sadori et al. (2016). MPT – Mid-Pleistocene Transition

The boundaries of the six magnetozones are treated as fixed tie-points to allow the placement of the stratigraphic and palaeoenvironmental record in chronostratigraphic context (Figure 11a). In the absence of higher resolution or absolute chronostratigraphic constraints within these magnetozones, the stratigraphy within them is linearly interpolated according to the average sedimentation rates to meet the time-depth relationship of the G4 borehole and surrounding stratigraphy (Figure 11b). The uncertainty within the individual magnetozones is mitigated by the spacing of palaeomagnetic samples and their corresponding reversals, which means the chronostratigraphic resolution is greatly increased from previous studies in the Early-Mid Pleistocene stratigraphy onshore the Gulf of Corinth. As a result, we tentatively propose a new age model (Figure 11b). The duration of the magnetozones means linear interpolation covers a variety of timespans, from roughly ~ 2 kyr for the Santa Rosa Chron (Yang et al., 2004) through to ~160 kyr for MAG 4 from the Santa Rosa Chron to the Brunhes-Matuyama boundary, and a mean magnetozone duration of 75 kyr. This spacing of tie points governing linear interpolation is similar to that of many geological, coarser resolution climatic stratigraphic studies (e.g. examining variability on 10^4-10^6 yrs timescales) in complex stratigraphy (e.g. 20-60 kyr ^{10}Be cosmogenic nuclide dating in D’Arcy et al., 2017; ~70 - 500 kyr δ^{13}C and biostratigraphy in Castelltort et al., 2017; 50-100 kyr biostratigraphy in Sømme et al., 2019). A linear interpolation between the magnetic tiepoints in the absence of other chronostratigraphic data is favoured over a ‘peak matching’ of different resolution palynological records or sequence stratigraphic interpretations as stratigraphic surfaces within rift basins are commonly complex and diachronous due to interactions of local accommodation and supply variations (Gawthorpe et al., 1994; Rohais et al., 2008; Muravchik et al., 2018; Barrett et al., 2018, 2019). As a result, stratigraphic surfaces are placed honouring their interpolated magnetostratigraphic position rather than through a correlative interpretation with global sea-level or vegetation records. The chronostratigraphic resolution provided by the magnetostratigraphy and the correlation to deltaic stratigraphic architecture (Cullen et al., 2020) provides a marked improvement on the existing age-range of the West Xylokastro RDF and means previous stratigraphic interpretations can be complemented with potential palaeoenvironmental triggers. Given the range of the magnetozone from the Santa Rosa chron (0.932 Ma) to the Brunhes-Matuyama reversal (0.773 Ma) and the quasi-instantaneous emplacement of the MTD, the positioning of WX7 and the MTD remains highly uncertain. Table 1 summarises the previously proposed interpretation of surfaces, and the chronostratigraphic placement as a result of this study.

Surface	Proposed Interpretation (Cullen et al., 2020)	Chronostratigraphic position (Figure 11)
Surface 2 (Base WX2)	Forced regressive surface documented by widespread erosion in Ilias delta and increase in conglomeratic lithofacies	~1.01 Ma within MIS28 global sea-level fall **or** ~1.03 Ma at onset of MIS 29 global sea-level rise
Surface 3 (Base WX3)	Forced regressive surface documented by widespread erosion and chutes in Ilias delta and continued coarse-grained lithofacies	~0.99 Ma during MIS28 at onset of global sea-level fall from MIS28 interstadial
Surface 4 (Base WX4)	Transgression documented by a back-stepping of delta foresets in the Ilias Delta and basin-wide dominance of mudstone-dominated stratigraphy	~0.96 Ma (MIS 26) during maximum rate of global sea-level rise to MIS 25
Surface 5 (Base WX5)	Maximum flooding surface marked by basinward downlap capping retrogradation of mudstone-rich WX4 stratigraphy	~0.95 Ma (MIS 25) during onset of global sea-level fall from MIS 25
Surface 6 (Base WX6)	Regressive surface documented by erosion in the Ilias delta and increase in conglomeratic lithofacies	~0.93 Ma (MIS 24) during highest rate of global sea-level fall to MIS 24
Surface 7 (Base WX7)	Possible transgressive surface, but weakly expressed as backstepping bottomsets onlapping onto foresets in Ilias delta	~0.91 – 0.87 Ma Highly uncertain due to MTD at G4 borehole

Table 1: Chronostratigraphic placement of key stratigraphic surfaces proposed in Cullen et al. (2020)

Coarse-grained delivery to the West Xylokastro Fault Block occurs during WX2, WX3, WX5, WX6 and WX7 (Figure 11, Figure 12). The character of these coarse-grained units varies; WX2 is dominated by conglomeratic sheets and sand-rich weakly channelised lobe deposits; WX3, is less conglomeratic with more heterolithic stratigraphy but is dominated by sand-rich channelised lobe and sheet-like deposits. WX5, WX6 and WX7 show sandstone-rich, but heterolithic sheet-like and weakly channelised deposits and more substantial conglomeratic channels interbedded with laterally discontinuous (<300 m) mudstones (Cullen et al., 2020). WX7 is eroded into by conglomerate-filled channels in locations close to the basin-bounding fault (Cullen et al., 2020). The widespread absence of coarse clastic delivery during WX1 and WX4 compared to WX2 and WX3 (and the variability within WX6 and WX7) highlights variability in sedimentary parameters.

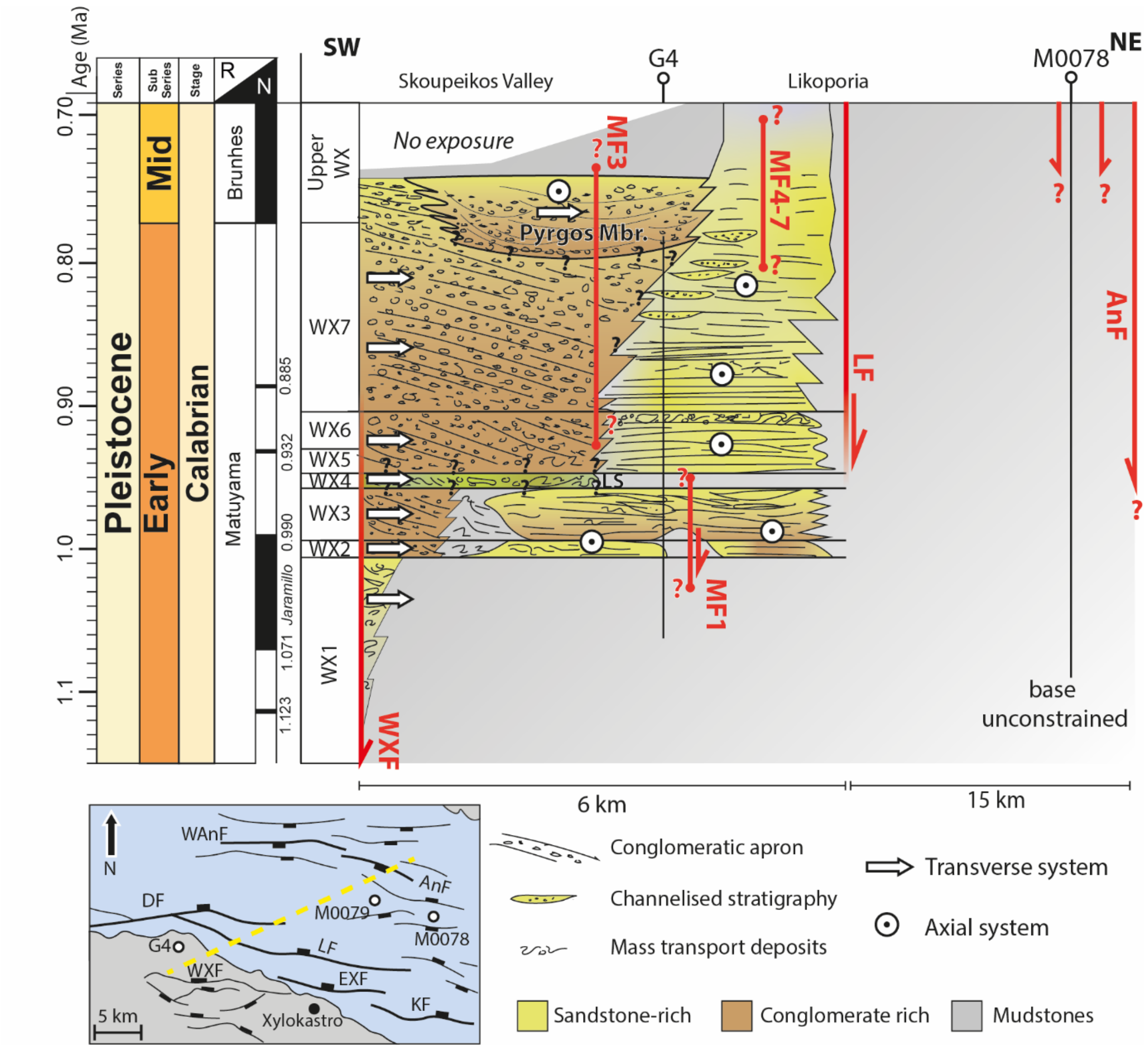

Figure 12: Schematic chronostratigraphic summary diagram for the central part of the for West Xylokastro to central Corinth rift region for the Early-Mid Pleistocene. WXF – West Xylokastro Fault, MF1-7 – Minor Fault, LF – Likoporia Fault, AnF – East Antikyra Fault, WAnF – West Antikyra Fault, EXF – East Xylokastro Fault, KF – Kiato Fault, DF – Derveni Fault. G4 – Syn-Rift Systems borehole, M0078, IODP Exp 381. Boreholes. The yellow dashed line approximates the location of the section, which condenses considerable lateral variability.

The absence of WX2 conglomerates in the G4 borehole reflects a structurally-controlled depositional variability. Elsewhere (Figure 2,3) this is a period of conglomerate delivery to the deep-water. Tzedakis et al. (2006) and Wagner et al. (2019) document arboreal pollen at Tenaghi Philippon measured at periods of time equivalent to pre-, syn- and post-WX2, which is in good agreement with the G4 record (~60% at the onset of MIS 28 compared to 60 - 65 % in Tenaghi Philippon, Figure 11). In the absence of intra-WX2 palaeoenvironmental information, correlation with the Tenaghi Philippon record indicates that this period of coarse-clastic delivery is coincident with reductions of 80 - 40 % in arboreal pollen at Tenaghi Philippon associated with the lowstand of the early MIS 28 stadial (Tzedakis et al., 2006, Figure 11). Given the limited volume of sediment exposed as a result of base-level fall in narrow shelved active margins (Collier et al., 2000), an increase in sediment supply as a result of deforestation in the catchment is considered a possible trigger for the change from mudstone dominated WX1 to conglomeratic WX2 in MIS 28. A decrease in forest cover acts to increase erosion and sediment discharge due to more limited physical creep processes such as rainsplash and dry ravel to export material previously stored within the catchment (e.g., from freeze-thaw weathering and other glaciogenic processes) (Bosch & Hewlett, 1982; Leeder et al., 1998; Istanbulluoglu & Bras, 2005).

Much of WX3 was deposited during times when catchments contained limited forest cover and steppic/shrubland vegetation similar to many Mediterranean glacials (e.g. MIS 24, 26, 28 - Tzedakis et al., 2006; Joannin et al., 2007a, b, 2008; Wagner et al., 2019). However, the interpolation between magnetostratigraphic tie points suggests the onset of WX3 was during an interstadial, with moderately developed forest and an affinity towards temperate forested biomes (Figure 11, 13b). Given the highly erosive nature of Surface 3 in the Ilias fan delta, and the significant thickness (~25-30 m) of the overlying WX3 stratigraphy downdip in the WXFB, we interpret that Surface 3 likely represents the onset of a minor interstadial to stadial base-level fall, the deep-water expression of which separates compensationally stacked WX2 and WX3. The presence of steppic elements in the middle part of WX3 is synchronous with a reduction in affinity to forested biomes. A less forested landscape could have acted to increase lowland-derived ‘soft’ sediment yield (e.g. soils, reworked trapped sediment) to maintain sediment delivery during the likely limited lowstand/base-level fall and aid progradation of the reworked shoreline (*sensu* Leeder et al., 1998, Figure 13c). In addition, we interpret high levels of precipitation evidenced by well-maintained aquatic element taxa and reed grasses (*Phragmites* sp.) (Figure 10,11,13b).

WX4 is preceded by a substantial expansion in forest cover to the highest level seen in the G4 stratigraphy (Figure 11, 13) and within the Tenaghi Philippon record (Tzedakis et al., 2006). The chronostratigraphic model suggests that this is synchronous with the global marine sea-level rise and warming related to the MIS 25 interglacial (Figure 11). During the warming phase of MIS 25, ~60% arboreal pollen values in the pollen sample at the base of WX4, and ~75% immediately prior to WX4 document this expansion, which is demonstrated through the strongest affinities to broad-ranging and temperate/warm, malacophyll prone forest biomes (e.g. CENF, COOL, TEDE, CMIX, ENWD in Figure 10). The strongest of these affinities tends towards CMIX, which may indicate a milder climate than the previous dominant GRAM and weak affinity to CMIX within the middle part of WX3. WX4 in the Ilias fan delta is recognised by a back-stepping relationship and fining upward indicative of delta retrogradation (Cullen et al., 2020). With WX4 chronostratigraphically constrained, we interpret the substantial magnitude and rate of this global marine transgression may have been mimicked by a more minor lake-level rise in Lake Corinth. Any lake level rise would likely have been amplified by ongoing subsidence, and we interpret this outpaced a synchronous reduction in sediment supply triggered by the expansion of catchment forest cover.

In the Ilias fan delta, WX4 is downlapped by prograding foresets of WX5 (Cullen et al., 2020). The chronostratigraphy and palynology of this study highlights this is coincident with a reduction in arboreal pollen during the latter part/peak of the MIS 25 interglacial highstand within WX5. Arboreal pollen percentages are reduced to 20% at the onset of WX5 and ~30% (20% of which is mesothermal) at the end of WX5. Biome affinities reflect this through showing stronger affinities to warm forest biomes

(TEDE, CMIX, ENWD), an increase in arid shrubland affinities, and strong affinities to grasslands. This contrasts with the maintained, and substantial, forest cover (75-90% arboreal pollen) in the Tenaghi Philippon Record (Tzedakis et al., 2006), although a similar reduction appears within the transition from MIS 25 to MIS24 that is younger than the linear interpolation at G4 suggests. Pollen samples within WX5 show the development of steppic and halophilic elements but an absence of cold, or humidity demanding, taxa such as *Abies.* This is similar to very warm/semi-arid episodes observed in severe interglacials in Early-Mid Pleistocene stratigraphy of Rhodes, Greece (Joannin et al., 2007b). The dominance of *Spiniferities* spp. through WX5 and WX6 appears concomitant with proposed base-level changes (Section 6) but cannot be used alone as an indicator of marine connection or lake-level control (cf. Morzadec-Kerfoun, 2005). However, such dinoflagellate variability is consistent with the influx of nutrients from increased terrigenous supply (Mudie et al., 2010). The reduction in arboreal pollen percentage in the West Xylokastro record is substantially larger (a reduction of 50-65%) than the higher frequency variability (75% +/- 10-15%) in the Tzedakis et al. (2006) record at this time and supports a genuine deforestation in the catchment rather than aliasing of higher-frequency variability. Therefore, we interpret that the reduction in forest cover (during a drier or semi-arid period of an interglacial) permits sediment supply increase to drive progradation of the Ilias fan delta and supply of sediment to the deep-water (Figure 11).

WX6 in the Ilias fan delta is marked as a subtle increase in the conglomerate fraction, whilst in other portions of the delta bottomset WX6 is marked by channelised features (Section 2, 4.1, Rubi et al., 2018, Cullen et al., 2020). Distally, Surface 6 (base WX6) does not record an increased coarse-grained proportion or major facies change from WX5 as it does more proximally. Surface 6, underlying WX6, in the linear age model likely occurs during the global cooling from MIS 25 to MIS24. In the G4 stratigraphy, arboreal pollen percentages increase at the proposed onset of WX6, which may have acted to coincidentally inhibit sediment supply from the catchment (Figure 11). This may explain why any coincident lake-level fall is not strongly represented in the stratigraphy. The sample at the top of WX6 shows a decrease in arboreal pollen percentages to assemblages more typical of Mediterranean glacials, dominated by grassland and steppe with limited development of forests that may have increased or maintained sediment supply to produce sandstone-dominated stratigraphy distally (Figure 10, 11). The G4 pollen record becomes sparse in WX7, which is more heterolithic and variable than underlying units (Cullen et al., 2020). However, the poor recovery of pollen in samples within WX7, and sparse spacing of samples due to the MTD at the basal part of WX7, means it is not possible to pose suitable interpretations on this part of the record.

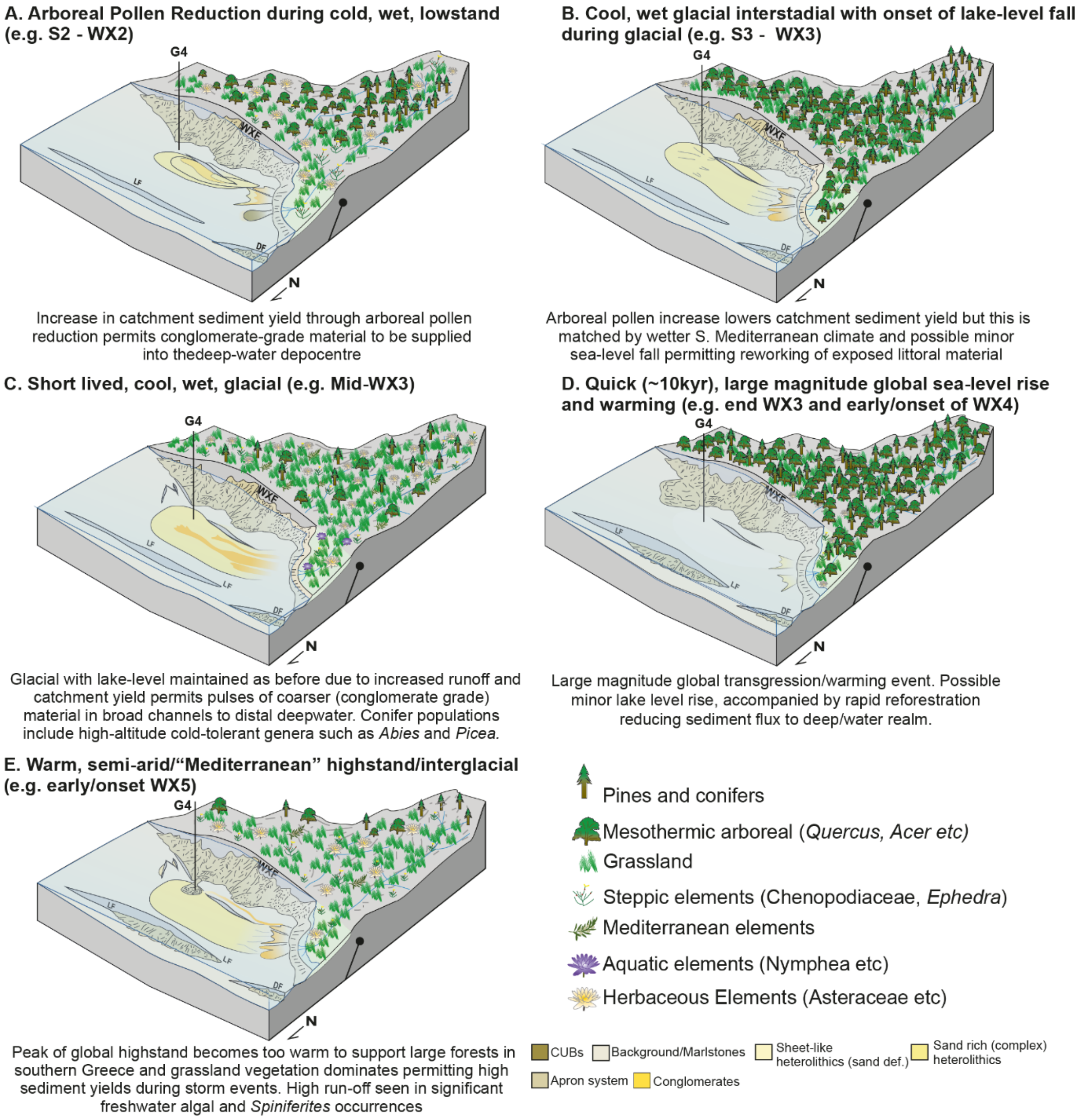

Figure 13: Conceptual cartoons highlighting vegetation and climatic variability and the impact of this on the timing and calibre of sediment delivered to the deep-water realm. WXF - West Xylokastro Fault, LF - Lykoporiá Fault, DF - Derveni Fault, CUBs - Convex Up Bodies (Cullen et al., 2020).

Stratigraphic and palynological observations highlight that climatic and vegetation variability likely impacted sediment delivery to the deep-water in the WXFB. None of the studied section is deposited under fully marine conditions, and hence lake-level is mostly a function of local climate and hydrology. However, we cannot exclude the possibility that minor marine incursions occured during part or parts of the broader transition from Lake Corinth, through to a temporarily marine-connected gulf by the Late Pleistocene (Collier, 1990; de Gelder et al., 2019; Gawthorpe et al., 2018; McNeil et al., 2019). The complex palaeogeography of Lake Corinth during the Early-Mid Pleistocene likely means that at West Xylokastro any marine signal could be weak if there were times when the lake became a strongly restricted embayment for example. We await further investigations from IODP 381 to characterise this transition in greater detail. Coarse-grained input is coincident with open vegetation typical of glacial conditions, or reduced forest cover in semi-arid interglacials. Severe supply reductions produce laterally extensive mudstone intervals during widespread increases in forestation, which may be coincident with high magnitude, rapid, 100-kyr paced warming events and global sea-level rises. Minor increases (those typical of interstadials or less severe, 41-kyr paced interglacials) appear to have a more limited impact on supply to the deep-water, producing subtle facies changes, which are not readily distinguished from autogenic facies variability. Given the limited duration (~40 kyr) of the change to mudstone dominated WX4 and the return to coarse-grained WX5 this perturbation to sediment supply is considerably shorter than longer-term variability in subsidence (e.g. Scholz, 2010; McNeil et al., 2019). As such we do not interpret that it could result from a subsidence ‘pulse’. At this, 10^4 yrs timescale subsidence is largely treated as gradually increasing through the averaging of millennial to centennial clustering of seismicity (e.g. Whittaker et al., 2011, 2010)

7.2 Topographic and temporal complexity in Early-Middle Pleistocene rift-margin catchments – implications and potential for further palynological investigations

7.2.1 Topographic complexity of short, steep drainage catchments

Early-Mid Pleistocene palaeogeographies of the Olvios catchment indicate approximately 1600 m of elevation difference from the uppermost hinterland to the topsets of the Ilias fan delta over ~15-18 km horizontal distance (Gawthorpe et al., 2018). This elevation difference covers a wide variety of Mediterranean vegetation biomes within the transportable distance offshore for airborne pollen (Capraro et al., 2005, Suc & Popescu, 2005; Beaudouin et al., 2007; up to 100 km for Pinaceae Szczepanek et al., 2017; Papadopolou et al., 2018; Marinova et al., 2018). This means the palynological assemblage is an aggregate of this spatial variability, which can inform detailed palaeoecology of the syn-rift hinterland (McArthur et al., 2016c), rather than an isolated local palynological signature (e.g. from very broad lowlands unrepresentative of larger catchments). In syn-rift catchments, this configuration can substantially impact the calibre and timing of sediment supply. For example, altitudinal increases in catchment forest cover can inhibit erosion in the upper reaches, whereas lowland deforestation in lower reaches can promote reworking ‘soft’ sediment yield from soils (Leeder et al., 1998). It is for this reason that the biomization and biome affinities are not treated as a singular confident biome affinity, but that similarly-high affinities or changes in affinity may be representative of the entire variability of catchment vegetation (Marinova et al., 2018). Additionally, we expect the impact of any temporary storage of pollen grains in the catchment to be limited in influencing our results through reworked pollen grains, due to the bulk of pollen transport being by wind, rather than fluvial input (Beaudoin et al., 2007) and the commonly corroded appearance of likely reworked grains. Deep-water syn-rift localities are likely to offer opportunities to test or investigate the potential for whole-catchment variability further due to the large range of elevations over relatively short catchments, which are within the range to receive pollen as a palaeoclimatic archive. This is contrary to offshore passive margin studies, which may receive pollen largely from extensive (> 100s km) lowlands that may only represent a small part of the larger fluvial catchments controlling offshore sediment supply.

7.2.2 Climatic variability and fluctuations of Lake Corinth in the Early-Middle Pleistocene

The Gulf of Corinth's location within the eastern-central Mediterranean places it within a transition from Atlantic-influenced Mediterranean climates (hot, dry summers and cool, wet and stormy winters) to an Eastern Mediterranean/Levant semi-arid/arid climate. Global climatic variability through the Pleistocene can either enhance or dampen the influence of either of these climatic regimes through latitudinal shifts of the Atlantic Westerly jet stream (COHMAP Members, 1988; Harrison et al., 1992; Leeder et al., 1998; Collier et al., 2000). Particularly severe interglacials may alter the typical latitudinal range of the Atlantic Westerly jet stream allowing a departure from the typically temperate, forest-dominated interglacials (Leeder et al., 1998; Tzedakis et al., 2006; Joannin et al., 2007a, b; Francke et al., 2016; Sadori et al., 2016; Lacey et al., 2016; Wagner et al., 2019). This may explain fluctuations between wet and dry interglacials observed in comparative studies between the Eastern and Western Mediterranean, particularly through the Early-Middle Pleistocene transition (Capraro et al., 2005; Suc & Popescu, 2005). Furthermore, the impact of this upon local hydrology and catchment vegetation for lakes makes estimating lake-level for Lake Corinth during the Early-Pleistocene challenging. Whilst many Pleistocene lake-level records are observed to vary in-phase with global marine eustatic variability such as Lakes Tana and Tanganyika, East Africa (Gasse et al., 1989; Marshall et al., 2011), local hydrological and climatic variations can alter the evaporation to precipitation ratio for a given water body to produce lake-levels that operate out-of-phase with global marine changes (Leeder et al., 1998). For instance, lake-level falls during interglacials are documented in Late Pleistocene and Holocene Eastern Mediterranean and Levant lakes on account of more evaporative, arid conditions (Torfstein et al., 2013; Kiro et al., 2017). Conversely, Gulf of Corinth lake levels in the Late Pleistocene are suggested to be in phase with global marine variability through highstand marine incursions (Collier, 1990; Armijo et al., 1996; McNeil et al., 2019a). However, there is limited independent control on lake-level during the Early-Middle Pleistocene, when the Gulf of Corinth was largely isolated (Gawthorpe et al., 2018; McNeill et al., 2019a). We observe retrogradation of the Ilias fan delta during WX4 (Cullen et al., 2020), which the magnetostratigraphy of this study suggests developed synchronously with a substantial eustatic global sea-level rise outside Lake Corinth to the MIS25 interglacial highstand (Figure 11, Section 7). The closed western end of Lake Corinth during the Early-Mid Pleistocene by the Rodini fluvial and deltaic systems means any marine incursions, if present, would have to come from the east of the study area (Ford et al., 2016; Gawthorpe et al., 2017; 2018; Somerville et al., 2020). However, any Early-Mid Pleistocene succession on the Corinth Isthmus that might record this interval has yet to be documented (Collier, 1990). Any alternative complex connection through the Megara Basin is poorly constrained due a limited age model (Bentham et al., 1991). These observations suggest that Lake Corinth levels may have operated (at least partly) in-phase with global marine variability at this time. An in-phase lake-level variability for the Gulf of Corinth is reasonable given that many of the catchments were affected by montane glaciations during the Pleistocene, particularly in the west of the rift (Pope et al., 2017; Hughes & Woodward, 2017, Leontaritis et al., 2020). Therefore, they would have been subject to increases in discharge from glacier melting, in the transition from glacials to interglacials, or reductions in discharge during glacier growth in glacials. The extent to which this was modified by higher overall precipitation during glacials (Leeder et al., 1998; Collier et al., 2000) is unclear, and may explain the minor absolute magnitude (10-15 m) of lake-level variability derived by Barrett et al. (2019) and de Gelder et al. (2019)

for the Early Pleistocene Gulf of Corinth compared to time-equivalent global sea level variability (50 – 100 m).

7.3 Early-Middle Pleistocene sediment supply variability in the West Xylokastro Fault Block

The typical climatic model for the Mediterranean is that highest sediment supply occurs during glacials, with limited supply to the basin during interglacials due to reduced precipitation and the trapping of sediment within the catchment because of well-developed forest cover (Leeder et al., 1998; Collier et al., 2000; Tzedakis et al., 2006; Sømme et al., 2011). In the deepest observed part of the WXFB, stratigraphy within WX2 and WX3 contains conglomerate, and gravel-rich lithofacies. The magnetostratigraphy suggests this was probably deposited during the glacial MIS 28 (Figure 11, Figure 13, Figure 14B, C). Coarse sediment supply is also maintained in WX5 and WX6, which is proposed to be during the latter part of the MIS25 interglacial. Although sandstone-dominated, WX5 and WX6 are more heterolithic than WX2 and WX3. In contrast, sediment supply and resultant grain-sizes are substantially reduced within WX4, interpreted to have occurred during the warming and transgression to the MIS 25 interglacial (Figure 11, Figure 13, Figure 14A, D). Frequent winter storms during subsequent glacials may help to flush-out sediment stored in catchments, aided by steppe-like vegetation that is less effective at trapping sediment within the catchment (Leeder et al., 1998; Marston 2010; Schmid et al., 2018). Alternatively, an interglacial-driven supply model has been proposed to explain examples of larger sediment volumes deposited in interglacials (e.g. Watkins et al., 2018). Here *larger* winter storms occur during interglacials on account of elevated ocean and atmospheric temperatures and carry out significant geomorphic 'work' in steep, short catchments, such as those surrounding the Gulf of Corinth (Trenberth et al., 2003; Berg et al., 2013; Bates et al., 2014; Watkins et al., 2018; Wagner et al., 2019). The MIS 25 interglacial in the Gulf of Corinth may represent an alternative form of Mediterranean interglacial (Figure 13e), proposed to have semi-arid lowland vegetation and partly forested mountains during its peak, contrary to typical widespread forest cover of most Pleistocene interglacials (Tzedakis et al., 2006; Joannin et al., 2007a,b; Figure 13d, 14a,d,e). In the G4 borehole record, well-developed forest is only seen during the preceding warming phase. Samples within MIS25 reveal substantially reduced Pinaceae pollen counts. The reduction in forest cover during the latter stages of the interglacial, coupled with large winter storms may well allow sediment flux to deep-water environments sooner than predicted by previous models (cf. Leeder et al., 1998).

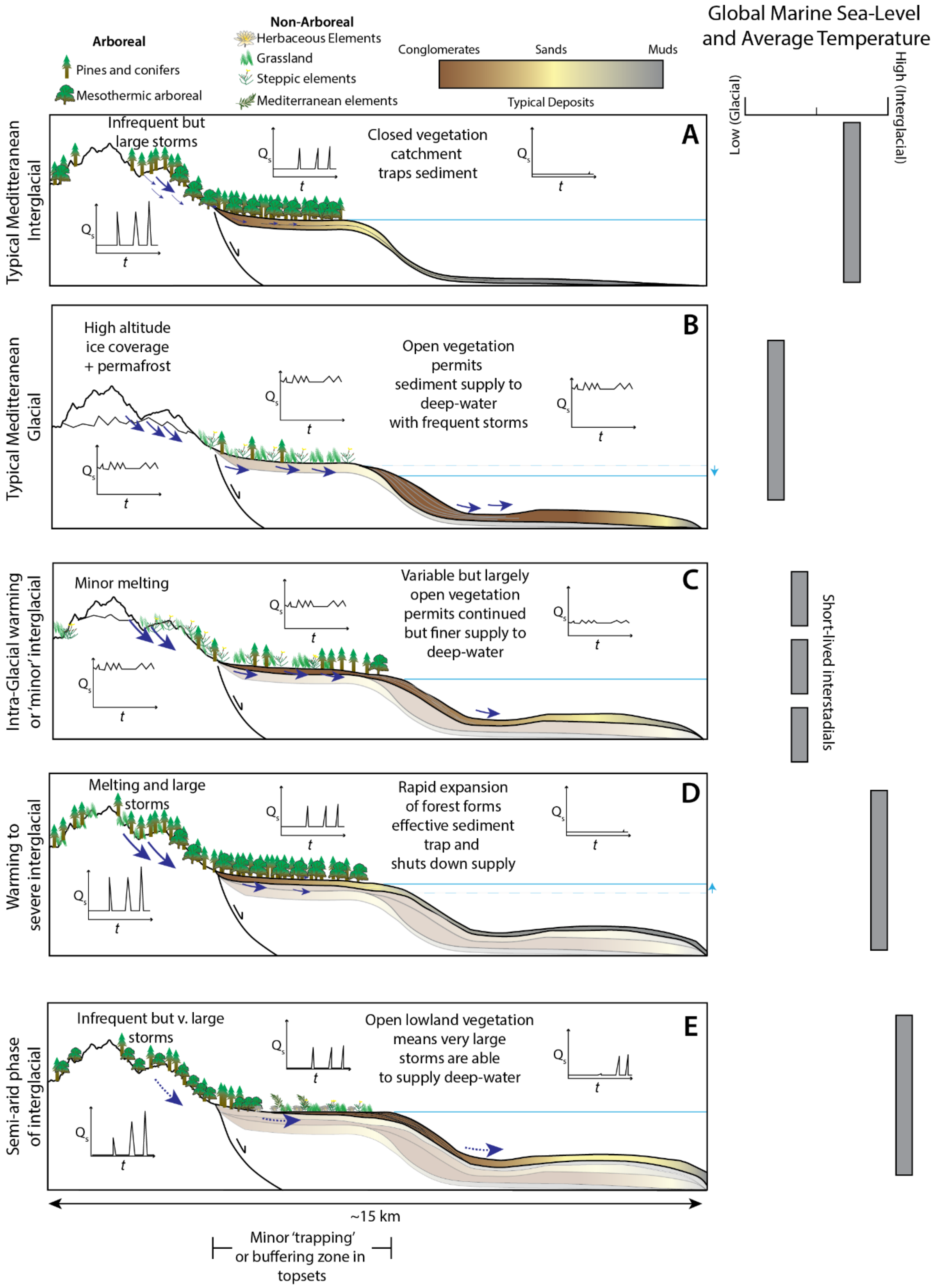

Figure 14: Conceptual cartoon models for sediment supply variability with Pleistocene climatic and vegetation changes in Mediterranean catchments.

The proposed climate during the peak of the atypical MIS25 Mediterranean interglacial is interpreted to have permitted enhanced sediment supply from catchments. The prevalence of nutrient-rich freshwater indicators like *Bottryococcus* and Spiniferites spp. in this part of the stratigraphy supports an interpretation of periods of high freshwater discharge into the basin (Mudie et al., 2010). Large storms, in cool, rather than very cold, wet winters may have eroded substantial volumes of sediment on dominantly grassland and xeric shrubland landscapes. Dry, hot summers are then interpreted to produce limited sediment delivery to the deep-water leading to highly seasonal sediment flux. This seasonal sediment delivery may explain the more heterolithic, but still coarse-grained, character of interglacial/highstand units like WX5 even where overall fluvial discharge may be considered lower in some models (e.g. Leeder et al., 1998), due to the increased erodibility of the landscape, and highly seasonal climates. This is similar to sediment delivery in the modern Gulf of Corinth, demonstrated by the frequency of subaqueous cable breaks basinward of river mouths concentrated during winter months following large storms (Heezen et al., 1966; Papadopoulos, 2003). Interglacials within the Quaternary vary in severity and associated with entirely different weather patterns (e.g. jet-stream positions, Harrison et al., 1992) producing variable climate conditions for a given interglacial or glacial. It is therefore recommended that interglacials, whilst warmer than their preceding or following glacial, are not by default treated as drier overall and should include the possibility of enhanced or reduced seasonality compared to other glacials or interglacials (e.g. Collier et al., 2000; Sømme et al., 2011).

Glacial periods of the Pleistocene in central Greece were often accompanied by montane glaciations (Smith et al., 1997; Hughes et al., 2006, 2007; Bathrellos et al., 2017; Hughes & Wooodward, 2017; Leontaritis et al., 2020). Whilst most of the Olvios drainage is unlikely to have suffered severe or full glaciation given its elevation below the equilibrium line for Pleistocene glaciations, extensive permafrost was likely, especially in its upper reaches (Hughes & Woodward, 2017; Leontaritis et al., 2020). In addition to colder temperatures, permafrost can further inhibit widespread forest growth during glacials which may promote increases in sediment transport out of the catchment (Woodward et al., 1992; Hughes et al., 2007). However, any deforestation competes with the ability for longer-term ice or permafrost coverage in the upper reaches of catchments to diminish supply by reducing the effective size of the catchment or restricting erodibility compared to an unglaciated catchment (Armitage et al., 2011; Romans et al., 2016; Watkins et al., 2018). The extent to which this impacts a catchment may be minor, with seasonal freeze-thaw weathering identified as the primary mechanism through which enhanced erosion during Mediterranean glacials occurs (Italian Apennines – Tucker et al., 2011). The sediment produced through this can be flushed-out of the catchment during minor warming or wet episodes in stadials, or the end of the glacial (Figure 13a, Figure 14b,c: Hughes et al., 2007; Armitage et al., 2011; Sømme et al., 2011; Tucker et al., 2011; Strachan et al., 2013; Cordier et al., 2017; Cao et al., 2018).

Ultimately, interglacially-driven supply relies on large, basin-drainage changes being recorded as a ‘step-change’ in stratigraphy (Armitage et al., 2011, Watkins et al., 2018). In contrast, glacially-driven supply relies on the consistency and averaging effect of frequent storms, and absence of forest cover common to Mediterranean glacials (Harrison et al., 1992, Collier et al., 2000). The climatic transition *between* glacials and interglacials has been poorly documented in deep-water syn-rift systems, with a focus on prevailing interglacial or glacial conditions. However, the nature of the transitions between interglacials and glacials are seen to be equally as important in interrupting sediment delivery from terrestrial catchments as lowstand/glacial or highstand/interglacial climate/vegetation conditions themselves (Sømme et al., 2011; Armitage et al., 2013). We interpret that both deforestation-aided glacial supply and highly seasonal interglacials increases in sediment supply were active in the Early-Mid Pleistocene WXFB.

7.4 Palaeoenvironmental controls on deep-water syn-rift sedimentation

The WXFB stratigraphy highlights that major climatic changes during global warming from glacials to severe interglacials may form a principal mechanism for inhibiting otherwise sustained sediment supply to the deep-water in rift settings. However, to expect all systems to respond similarly may be unrealistic given well-documented examples of the transition to interglacials providing increased sediment supply through deglaciation of drainage catchments (e.g. Mississippi Fan Delta during Holocene transgression (Covault & Graham, 2010) and Armorican turbidite systems during the Last Glacial (20-15ka) warming (Toucanne et al., 2012)). The manner in which a landscape and basin responds to changes from glacials to interglacials will be specific to a given landscape and rely on local interaction and feedbacks between drainage physiography, the rate and nature of climatic and vegetation variability, oceanographic changes and shoreline processes (Sømme et al., 2011; Dixon et al., 2012; Armitage et al., 2013; Hay et al., 2014; Bernhardt et al., 2016, 2017; Beckers et al., 2016; Romans et al., 2016; Rovere et al., 2016; Horsch & Fourniotis, 2018; Watkins et al., 2018; Pechlivanidou et al., 2018; Cosgrove et al. 2018).

In the WXFB, it appears only the largest climatic changes produce widespread and major stratigraphic changes. WX4, represents a temporary system-wide shut-down of sediment supply that we propose to be synchronous with MIS 25 a major global warming episode, and is the only major mudstone succession in an otherwise coarse-grained dominated succession. Other, less severe, warming events in the Early-Mid Pleistocene appear to have limited impact upon the stratigraphy. Ultimately, this results in intra-formational and laterally extensive mudstone-dominated successions being rare amongst sustained coarse-grained supply, but where present are typically triggered by rapid and extensive forestation related to warming during the transition from glacials to severe interglacials (Figure 13, 14). The extreme narrowness or absence of shelves and limited sediment storage in terrestrial settings along active rift margins permits enhanced sensitivity of the deep-water realm to major cessations and triggers of sediment supply in the catchments from climatic changes (Burgess & Hovius, 1998; Carvajal & Steel, 2006; Covault & Graham, 2010; Strachan et al., 2013; Romans et al., 2016; Harris et al., 2018; Watkins et al., 2018; Zhang et al., 2019a, b). Counterintuitively, small magnitude or high frequency (10^3 yrs) supply fluctuations may not be stratigraphically represented as reduced sedimentation, or changes in sedimentary parameters, because supply is readily maintained to the deep-water across narrow shelves within the response timescale of the landscape (Romans et al., 2016; Jobe et al., 2017; Hajek & Straub, 2017; Tofelde et al., 2021). More subtle changes may therefore be non-resolvable from bathymetrically controlled spatial patterns in deposition or autogenic variability. In the WXFB, where sediment supply is derived from the footwall catchment, high sediment supply across a narrow Gilbert fan delta topset (1.5 km long and ~3.5 km radius, Cullen et al., 2020) is interpreted to prevent the preservation of environmental signals of minor changes in climate or lake-level in the deep-water stratigraphy as changes of lithofacies. However, the lower subsidence rates and shallower water depths typical of a hanging wall dip-slope system, permit larger alluvial topsets or the development of low angle, subaqueous shelves (Gawthorpe et al., 1994; Collier & Gawthorpe, 1995, Henstra et al., 2016, cf. Figure 14). This increases the potential for sediment storage and signal-shredding (Jerolmack & Paola, 2010) along the transport path prior to the deep-water realm, which may act to enhance the impact of high-frequency, low-magnitude, minor sediment flux reductions contrary to the maintained supply observed in the West Xylokastro.

8 Conclusion

Deep-water syn-rift sediment delivery relies on the complicated interplay of climate, vegetation, drainage arrangement, shelf physiography, and structural evolution. ‘Classical’ sequence stratigraphic models, which predict delivery restricted to lowstands or base-level falls, do not sufficiently represent the variability in rift basin-fills. Typically, active rifts are dominated by narrow or absent shelves, and as such their deep-water environments are sensitive to onshore changes in sediment flux, which may be linked to climatic variability. Vegetation changes coherent with global, orbital-forced climatic variability in the Early-Mid Pleistocene favour increased sediment delivery during glacial periods, and during semi-arid highstands/interglacial periods when high sediment supply is aided by large interglacial winter storms and a reduction in lowland forest cover. Coherence between vegetation and climate is persistent during the obliquity-controlled Early Pleistocene. However, vegetation fluctuations occur at higher temporal orders and magnitudes following the Early-Mid Pleistocene transition to eccentricity-paced glacioeustasy. In the West Xylokastro Fault Block, deep-water syn-rift coarse-grained sediment delivery is only hindered during large magnitude warming events related to larger, eccentricity-paced transgressions, which promotes widespread forest cover that reduces catchment sediment yield. Where possible, different severities of glacial or interglacial episodes should be included in palaeoclimate models rather than binary, dry-interglacial vs. wet-glacial models. The role of highly seasonal or wet interglacials may be important for triggering sediment release from onshore catchments into the deep-water realm. The study highlights the variability of the stratigraphic signature of such signals, which can be interpreted using palynological data to discern palaeoenvironmental change despite the distal setting, and the typical coarse grain-size of the deep-water deposits in such systems. The study highlights the value of integrating chronostratigraphic interpretation with palynological and broader stratigraphic relationships to help discern the evolution of deep-water syn-rift systems and provides new conceptual models for climatic control on deep-water sediment delivery.

9 Acknowledgements

This publication forms part of the first author's PhD project which was funded by the Syn-Rift Systems (PETROMAKS 2) project funded by the Research Council of Norway (Project number 255229/E30) and industry partners Aker BP, ConocoPhillips, DNO, Equinor, Tullow Oil and Neptune Energy and by the University of Leeds. TC and RLG also acknowledge VISTA visitor and professorship funding and Equinor for core storage and viewing facilities in Bergen. Natasha Barlow is thanked for access to a Leica DM2500 microscope. Fanis Chatoupis of HydroGEO, and the chair of the council of Kalithea are thanked for facilitating drilling of the borehole in Greece. Al Fraser and Bill McCaffrey are thanked for discussions on an earlier version of this manuscript. Pollen plots were generated using C2 (https://www.staff.ncl.ac.uk/stephen.juggins/software/C2Home.htm). Palynological sample preparation by Malcolm Jones of Palynological Laboratory Services Ltd, Anglesey, Wales. We thank the reviewers along with the editor Brian Romans and Chief Editor Valero Acocella for their thorough and constructive reviews and handling of this manuscript.

10 References

Allen, P.A. 2008. Time scales of tectonic landscapes and their sediment routing systems In: K. Gallagher, S. . Jones and J. Wainwright, eds. *Landscape Evolution: Denudation, Climate and Tectonics Over Different Time and Space Scales. Geological Society of London Special Publication No. 296.* Geological Society London, pp.7–28.

Armijo, R., Meyer, B., King, G.C.P., Rigo, A. and Papanastassiou, D. 1996. Quaternary evolution of the Corinth Rift and its implications for the Late Cenozoic evolution of the Aegean. *Geophys. J. Int.* 126, pp.11–53.

Armitage, J.J., Duller, R.A., Whittaker, A.C. and Allen, P.A. 2011. Transformation of tectonic and climatic signals from source to sedimentary archive. *Nature Geoscience*. 4, pp.231–235.

Armitage, J.J., Dunkley Jones, T., Duller, R.A., Whittaker, A.C. and Allen, P.A. 2013. Temporal buffering of climate-driven sediment flux cycles by transient catchment response. *Earth and Planetary Science Letters.* 369–370, pp.200–210.

Armitage, J.J., Whittaker, A.C., Zakari, M. and Campforts, B. 2018. Numerical modelling of landscape and sediment flux response to precipitation rate change. *Earth Surface Dynamics*. 6, pp. 77-99.

Backert, N., Ford, M., Malartre, F., Architecture and sedimentology of the Kerinitis Gilbert-type fan delta, Corinth Rift, Greece. *Sedimentology*. 57. pp.543-586.

Barrett, B.J., Hodgson, D.M., Collier, R.E.L., Dorrell, R. 2018. Novel 3D sequence stratigraphic numerical model for syn-rift basins: Analysing architectural responses to eustasy, sedimentation and tectonics. *Marine and Petroleum Geology*. 92, pp. 270-284.

Barrett, B.J., Collier, R.E.L., Hodgson, D.M., Gawthorpe, R.L., Dorrell, R. and Cullen, T.M. 2019. Quantifying faulting and base level controls on syn-rift sedimentation using stratigraphic architectures of coeval, adjacent Early-Middle Pleistocene fan deltas in Lake Corinth, Greece. *Basin Research.* pp.1–26.

Bates, S.L., Siddall, M. and Waelbroeck, C. 2014. Hydrographic variations in deep ocean temperature over the mid-Pleistocene transition. *Quaternary Science Reviews*. 88, pp.147–158.

Bathrellos, G.D., Skilodimou, H.D., Maroukian, H., Gaki-Papanastassiou, K., Kouli, K., Tsourou, T. and Tsaparas, N. 2017. Pleistocene glacial and lacustrine activity in the southern part of Mount Olympus (central Greece). *Area*. 49, pp.137–147.

Beaudouin, C., Suc, JP, Escarguel, G., Arnaud, M. and Charmasson, S. 2007 The significance of pollen signal in present-day marine terrigenous sediments: The example of the Gulf of Lions (western Mediterranean Sea), *Geobios*, 40 (2), pp. 159-172

Beckers, A., Hubert-Ferrari, A., Beck, C., Bodeux, S., Tripsanas, E., Sakellariou, D. and De Batist, M. 2015. Active faulting at the western tip of the Gulf of Corinth, Greece, from high-resolution seismic data. *Marine Geology*. 360, pp.55–69.

Beckers, A., Beck, C., Hubert-Ferrari, A., Tripsanas, E., Crouzet, C., Sakellariou, D., Papatheodorou, G. and De Batist, M. 2016. Influence of bottom currents on the sedimentary processes at the western tip of the Gulf of Corinth, Greece. *Marine Geology.* 378, pp.312–332.

Bell, R.E., McNeill, L.C., Bull, J.M., Henstock, T.J., Collier, R.E.L. and Leeder, M.R. 2009. Fault architecture, basin structure and evolution of the Gulf of Corinth rift, central Greece*. Basin Research*. 21, pp.824–855.

Benninghoff, W.S., 1962. Calculation of pollen and spores density in sediments by addition of exotic pollen in known quantities. *Pollen et Spores* ,6, 332–333

Berg, P., Moseley, C. and Haerter, J.O. 2013. Strong increase in convective precipitation in response to higher temperatures. *Nature Geoscience*. 6(3), pp.181–185.

Bernhardt, A., Hebbeln, D., Regenberg, M., Lückge, A. and Strecker, M.R. 2016. Shelfal sediment transport by an undercurrent forces turbidity current activity during high sea level along the Chile continental margin. *Geology.* 44, pp.295–298.

Bernhardt, A., Schwanghar, W., Hebbeln, D., Stuut, J.-B. W., and Strecker, M.R. 2017. Immediate propagation of deglacial environmental change to deep-marine turbidite systems along the Chile convergent margin. *Earth Planetry Science Letters*. 473, pp. 190-204.

Beug, H.-J. 2015. Leitfaden der Pollenbestimmung für Mitteleuropa und angrenzende Gebeite 2nd ed. München: Verlag Dr. Friedrich Pfeil.

Blum, M.D. and Hattier-Womack, J. 2009. Climate Change, Sea-level change, and fluvial sediment supply to deepwater depositional systems In: B. Kneller, O. Martinsen and B. McCaffrey, eds. *External Controls on Deep-Water Depositional Systems SEPM Special Publication No.92.* Tulsa, OK: SEPM (Society for Sedimentary Geology), pp.15–39.

Bogaart, P.W., Van Balen, R.T., Vadenberge, J., Kasse, C. 2002 Process-based modelling of the climatic forcing of fluvial sediment flux: some examples and a discussion of optimal model complexity *in* Jones, S.L., Frostick, L.E., (eds.) *Sediment Flux to Basins: Causes, Controls and Consequences* Geological Society Special Publication 191, pp187-198.

Bourget, J., Zaragosi, S., Mulder, T., Schneider, J.L., Garlan, T., Van Toer, A., Mas, V. and Ellouz-Zimmermann, N. 2010a. Hyperpycnal-fed turbidite lobe architecture and recent sedimentary processes: A case study from the Al Batha turbidite system, Oman margin. *Sedimentary Geology*. 229(3), pp.144–159.

Bosch, J., Hewlett, J. 1982. A review of catchment experiments to determine the effect of vegetation changes on water yield and evapotranspiration. *Journal of Hydrology.* 55(1-4). pp. 3-23.

Bourget, J., Zaragosi, S., Ellouz-Zimmermann, S., Ducassou, E., Prins, M.A., Garlan, T., Lanfumey, V., Schneider, J.-L., Rouillard, P. and Giraudeau, J. 2010b. Highstand vs. lowstand turbidite system growth in the Makran active margin: Imprints of high-frequency external controls on sediment delivery mechanisms to deep water systems. *Marine Geology*. 274, pp.187–208.

Buckley, S.J., Ringdal, K., Naumann, N., Dolva, B., Kurz, T.H., Howell, J.A., Dewez, T.J 2019. LIME: Software for 3-D visualization, interpretation, and communication of virtual geoscience models. *Geosphere*. 15 (1), pp. 222-235.

Burgess, P.M. and Hovius, N. 1998. Rates of delta progradation during highstands: consequences for timing of deposition in deep-marine systems. *Journal of the Geological Society.* 155, pp.217–222.

Cande, S.. and Kent, D.. 1995. Revised calibration of the geomagnetic polarity timescale for the late Cretaceous and Cenozoic. *Journal of Geophysical Research.* 100, pp.6093–6095.

Cao, Y., Wang, Y., Gluyas, J.G., Liu, Huimin, Liu, Haining and Song, M. 2018. Depositional model for lacustrine nearshore subaqueous fans in a rift basin : The Eocene Shahejie Formation , Dongying Sag , Bohai Bay Basin , China. *Sedimentology.* 65, pp.2117–2148.

Capraro, L., Asioli, A., Backman, J., Bertoldi, R., Channell, J.E.T., Massari, F. and Rio, D. 2005. Climatic patterns revealed by pollen and oxygen isotope records across the Matuyama-Brunhes boundary in the central Mediterranean (southern Italy) *In:* M. Head and P. Gibbard, eds. *Early-Middle Pleistocene Transitions: The Land-Ocean Evidence. Geological Society London Special Publication No. 247* Geological Society London, pp.159–182.

Carvajal, C.R. and Steel, R.J. 2006. Thick turbidite successions from supply-dominated shelves during sea-level highstand. *Geology*. 34, pp.665–668.

Castelltort, S., Honegger, L., Adatte, T., Clark, J.D., Puigdefàbregas, C., Spangenberg, J.E., Dykstra,M.L., Fildani, A. Detecting eustatic and tectonic signals with carbon isotopes in deep-marine strata, Eocene Ainsa Basin, Spanish Pyrenees. 2017. *Geology*. 45 (8). pp. 707-710.

Causse, C., Moretti, I., Eschard, R. and Micarelli, L. 2004. Kinematics of the Corinth Gulf inferred from calcite dating and syntectonic sedimentary characteristics. *Comptes Rendus Geoscience*. 336(4–5), pp.281–290.

Channell, J.E.T 2017. Magnetic excursions in the late Matuyama Chron (Olduvai to Matuyama-Brunhes boundary) from North Atlantic IODP sites. *Journal of Geophysical Research: Solid Earth*, 122, pp.773-789.

Cheng, L., Zhang, L., Chiew, F.H.S., Canadell, J.G., Zhao, F., Wang, Y.P., Hu, X. and Lin, K. 2017. Quantifying the impacts of vegetation changes on catchment storage-discharge dynamics using paired-catchment data. *Water Resources Research.* 53(7), pp.5963–5979.

Chester, P.I. and Raine, J.I. 2001. Pollen and spore keys for Quaternary deposits in the northern Pindos Mountains, Greece. *Grana.* 40, pp.299–387.

Cohen K.M. & Gibbard, P. 2016 Global chronostratigraphical correlation table for the last 2.7 million years. V.2016a Subcommission on Quaternary Stratigraphy (International Commission on Stratigraphy), Cambridge, England.

COHMAP MEMBERS 1988. Climatic changes of the last 18,000 years:observ and model situations. *Science.* 241, pp.1043–1052.

Collier, R.E.L. 1990. Eustatic and tectonic controls upon Quaternary coastal sedimentation in the Corinth Basin, Greece. J*ournal of the Geological Society.* 147, pp.301–314.

Collier, R.E.L. and Dart, C.J. 1991. Neogene to Quaternary rifting, sedimentation and uplift in the Corinth Basin,Greece. *Journal of the Geological Society.* 148, pp.1049–1065.

Collier, R.E.L. and Gawthorpe, R.L. 1995. Neotectonics, drainage and sedimentation in central Greece: insights into coastal reservoir geometries in syn-rift sequences In: J. Lambiase, ed. *Hydrocarbon Habitat in Rift Basins, Geological Society Special Publication No. 80.* Geological Society of London, pp.165–181.

Collier, R.E.L., Leeder, M.R., Trout, M., Ferentinos, G., Lyberis, E. and Papatheodorou, G. 2000. High sediment yields and cool, wet winters: Test of last glacial paleoclimates in the northern Mediterranean. *Geology.* 28, pp.999–1002.

Cordier, S., Adamson, K., Delmas, M., Calvet, M. and Harmand, D. 2017. Of ice and water: Quaternary fluvial response to glacial forcing. *Quaternary Science Reviews.* 166, pp.57–73.

Cosgrove, G.I.E., Hodgson, D.M., Poyatos-Moré, M., Mountney, N.P. and McCaffrey, W.D. 2018. Filter Or Conveyor? Establishing Relationships Between Clinoform Rollover Trajectory, Sedimentary Process Regime, and Grain Character Within Intrashelf Clinothems, Offshore New Jersey, U.S.A. *Journal of Sedimentary Research.* 88(8), pp.917–941.

Covault, J.A. and Graham, S.A. 2010. Submarine fans at all sea-level stands: Tectono-morphologic and climatic controls on terrigenous sediment delivery to the deep sea. *Geology.* 38, pp.939–942.

Cullen, T.M, Collier, R.E.Ll, Gawthorpe R.L, Hodgson, D.M and Barrett, B.J. 2020. Axial and transverse deep-water sediment supply to syn-rift fault terraces: insights from the West Xylokastro Fault Block, Gulf of Corinth, Greece, *Basin Research,* 32, pp. 1105-1139

de Gelder, G., Fernández-blanco, D., Melnick, D., Duclaux, G., Bell, R.E., Jara-muñoz, J., Armijo, R. and Lacassin, R. 2019. Lithospheric flexure and rheology determined by climate cycle markers in the Corinth Rift. *Scientific Reports*. 9 pp.1–12.

Dixon, J.F, Steel, R.J, Olariu, C, 2012. Shelf-Edge Delta Regime as a Predictor of Deep-Water Deposition. *Journal of Sedimentary Research*, 82, pp. 681-687

Djamali, M and Cilleros, K. 2020. Statistically significant minimum pollen count in Quaternary pollen analysis; the case of pollen-rich lake sediments. *Review of Palaeobotany and Palynology*. 275. 104156. https://doi.org/10.1016/j.revpalbo.2019.104156.

Doutsos, T. and Poulimenos, G. 1992. Geometry and kinematics of active faults and their seismotectonic significance in the western Corinth-Patras rift (Greece). *Journal of Structural Geology.* 14, pp.689–699.

Fatourou, E., Kafetzidou, A., Panagiotopoulos,K., Marret, F., Papadopoulous,S., Kouli, K. and the IODP Expedition 381 Science Team. 2021. Quaternary Environmental Changes in the Corinth Rift Area: the IODP 381 Palynological Record. *EGU General Assembly 2021, EGU21-11360*

Fernández-Blanco D., de Gelder G., Lacassin R., and Armijo, R. 2019. A new crustal fault formed the modern Corinth Rift, *Earth-Science Reviews,* 19

Fernández-Blanco D., de Gelder G., Lacassin R., and Armijo, R. 2020. Geometry of flexural uplift by continental rifting in Corinth, Greece. *Tectonics*, 39, https://doi.org/10.1029/2019TC005685

Flotté, N., Plagnes, V., Sorel, D. and Benedicto, A. 2001. Attempt to date Pleistocene normal faults of the Corinth-Patras Rift (Greece) by U/Th method, and tectonic implications*. Geophysical Research Letters*. 28(19), pp.3769–3772.

Ford, M., Williams, E.A., Malartre, F. and Popescu, S.-M. 2007. Stratigraphic Architecture, Sedimentology and Structure of the Vouraikos Gilbert-Type Fan Delta, Gulf of Corinth, Greece *In*: I. Jarvis, G. Nichols, E. Williams and C. Paola, eds. *Sedimentary Processes, Environments and Basins, Special Publication of the International Association of Sedimentologists*., pp.49–90.

Ford, M., Rohais, S., Williams, E.A., Bourlange, S., Jousselin, D., Backert, N. and Malartre, F. 2013. Tectono-sedimentary evolution of the western Corinth rift (Central Greece). *Basin Research.* 25, pp.3–25.

Ford, M., Hemelsdaël, R., Mancini, M. and Palyvos, N. 2016. Rift migration and lateral propagation: evolution of normal faults and sediment-routing systems of the western Corinth rift (Greece) *In:* C. Childs, R. . Holdsworth, C. A.-L. Jackson, T. Manzocchi, J. . Walsh and G. Yielding, eds. *The Geometry and Growth Of Normal Faults - Geological Society Special Publications 439* Geological Society London, pp.131–168.

Francke, A, Wagner, B., Just, J., Leicher, N., Gromig, R., Baumgarten, H., Vogel, H., Lacey, J.H., Sadori, L., Wonik, T., Leng, M., Zanchetta, G., Sulpizio, R., Giacco, B. 2016. Sedimentological processes and environmental variability at Lake Ohrid (Macedonia, Albania) between 637 ka and the present. *Biogeosciences*, 13. pp. 1179-1196

Gasse, F., Lédée, V., Massault, M. and Fontes, J.C. 1989. Water-level fluctuations of Lake Tanganyika in phase with oceanic changes during the last glaciation and deglaciation. *Nature.* 342, pp.57–59.

Gawthorpe, R.L., Fraser, A.J. and Collier, R.E.L. 1994. Sequence stratigraphy in active extensional basins: implications for the interpretation of ancient basin-fills. *Marine and Petroleum Geology*. 11, pp.642–658.

Gawthorpe, R.L., Andrews, J.E., Collier, R.E.L., Ford, M., Henstra, G.A., Kranis, H., Leeder, M.R., Muravchik, M., Skourtsos, E. 2017. Building up or out? Disparate sequence architectures along an active rift margin – Corinth Rift, Greece. *Geology*. 45 (12). pp. 1111-1114.

Gawthorpe, R.L., Leeder, M.R., Kranis, H., Skourtsos, E., Andrews, J.E., Henstra, G.A., Mack, G.H., Muravchik, M., Turner, J.A. and Stamatakis, M. 2018. Tectono-sedimentary evolution of the Plio-Pleistocene Corinth rift, Greece. *Basin Research*. 30, pp.448–479.

Geurts, A.H., Cowie, P.A., Duclaux, G., Gawthorpe, R.L., Huismans, R.S., Pedersen, V.K., Wedmore, L.N.J. 2018. Drainage integration and sediment dispersal in active continental rifts: A numerical modelling study of the central Italian Apennines. *Basin Research*. 30. pp. 965-989.

Gobo, K., Ghinassi, M. and Nemec, W. 2014. Reciprocal Changes in Foreset to Bottomset Facies in a Gilbert-Type Delta: Response to Short-Term Changes in Base Level. *Journal of Sedimentary Research*. 84, pp.1079–1095.

Gobo, K., Ghinassi, M. and Nemec, W. 2015. Gilbert-type deltas recording short-term base-level changes: Delta-brink morphodynamics and related foreset facies. *Sedimentology*. 62, pp.1923–1949.

Gupta, S., Underhill, J.., Sharp, I.. and Gawthorpe, R.. 1999. Role of fault interactions in controlling synrift sediment dispersal patterns: Miocene, Abu Alaqa Group, Suez Rift, Sinai, Egypt. *Basin Research.* 11(2), pp.167–189.

Gutierrez-Pastor, J., Hans Nelson, C., Goldfinger, C., Johnson, J., Escutia, C., Eriksson, A. and Morey, A.. 2009. Earthquake Control of Holocene Turbidite Frequency Confirmed by Hemipelagic Sedimentation Chronology on the

Cascadia and Northern California Active Continental Margins In: B. Kneller, O. Martinsen and B. McCaffrey, eds. *External Controls on Deep-Water Depositional Systems SEPM Special Publication No. 92*. Tulsa, OK: SEPM (Society for Sedimentary Geology), pp.179–197.

Hadler-Jacobsen, F., Johannessen, E.P., Ashton, N., Henriksen, S., Johnson, S.D. and Kristensen, J.B. 2005. Submarine fan morphology and lithology distribution: A predictable function of sediment delivery, gross shelf-to-basin relief, slope gradient and basin topography *In:* Doré, A.G and Vining, B.A eds. *Petroleum Geology: North-West Europe and Global Perspectives - Proceedings of the 6th Petroleum Geology Conference*, pp.1121–1145.

Hajek, E.A. and Straub, K.M. 2017. Autogenic Sedimentation in Clastic Stratigraphy. *Annual Review of Earth and Planetary Sciences.* 45, pp.681–709.

Harris, A.D., Baumgardner, S.E., Sun, T. and Granjeon, D. 2018. A Poor Relationship Between Sea Level and Deep-Water Sand Delivery. *Sedimentary Geology*. 370, pp.42–51.

Harrison, S.P., Prentice, I.C. and Bartlein, P.J. 1992. Influence of insolation and glaciation on atmospheric circulation in the North Atlantic sector: Implications of general circulation model experiments for the Late Quaternary climatology of Europe. *Quaternary Science Reviews.* 11, pp.283–299.

Hay, C., Mitrovica, J.X., Gomez, N., Creveling, J.R., Austermann, J. and Kopp, R.R. 2014. The sea-level fingerprints of ice-sheet collapse during interglacial periods. *Quaternary Science Reviews*. 87, pp.60–69.

Heezen, B.C., Ewing, M. and Johnson, G.L. 1966. The Gulf of Corinth floor. *Deep-Sea Research and Oceanographic Abstracts*. 13, pp.381–411.

Henstra, G.A., Grundvåg, S.-A., Johannessen, E.P., Kristensen, T.B., Midtkandal, I., Nystuen, J.P., Rotevatn, A., Surlyk, F., Sæther, T. and Windelstad, J. 2016. Depositional processes and stratigraphic architecture within a coarse-grained rift-margin turbidite system: The Wollaston Forland Group, east Greenland. *Marine and Petroleum Geology*. 76, pp.187–209.

Horsch, G.M. and Fourniotis, N.T. 2018. On strong nearshore wind-induced currents in flow-through gulfs: Variations on a theme by Csanady. *Water.* 10, pp.1–14.

Hughes, P.D., Woodward, J.C. and Gibbard, P.L. 2006. Late Pleistocene glaciers and climate in the Mediterranean. *Global and Planetary Change*. 50, pp.83–98.

Hughes, P.D., Woodward, J.C. and Gibbard, P.L. 2007. Middle Pleistocene cold stage climates in the Mediterranean: New evidence from the glacial record. *Earth and Planetary Science Letters.* 253, pp.50–56.

Hughes, P.D. and Woodward, J.C. 2017. Quaternary glaciation in the Mediterranean mountains: A new synthesis *In:* P. D. Hughes and J. . Woodward, eds. *Quaternary Glaciation in the Mediterranean Mountains, Geological Society of London Special Publications No. 433*. Geological Society of London, pp.1–23.

Imbrie, J., Berger, A., Boyle, E.A., Clemens, S.C., Duffy, A., Howard, W.R., Kukla, G., Kutzbach, J., Martinson, D.G., McIntyre, A., Mix, A.C., Molfino, B., Morley, J.J ., Peterson, L.C., Pisas, N.G., Prell, W.L., Raymo, M.E., Shackleton, N.J. and Toggweiler, J.R., 1993. On the structure and origin of major glaciation cycles 2. The 100,000-year cycle. *Paleoceanography.* 8(6), pp.699– 735

Istanbulluoglu, E. and Bras, R.L. 2005. Vegetation-modulated landscape evolution: Effects of vegetation on landscape processes, drainage density, and topography. *Journal of Geophysical Research: Earth Surface.* 110, pp.1–19.

Jerolmack, D.J. and Paola, C. 2010. Shredding of environmental signals by sediment transport. *Geophysical Research Letters.* 37(19), pp.1–5.

Joannin, S., Quillévéré, F., Suc, J.-P., Lécuyer, C. and Martineau, F. 2007a. Early Pleistocene climate changes in the central Mediterranean region as inferred from integrated pollen and planktonic foraminiferal stable isotope analyses. *Quaternary Research*. 67, pp.264–274.

Joannin, S., Cornée, J.-J., Moissette, P., Suc, J.-P., Koskeridou, E., Lécuyer, C., Buisine, C., Kouli, K. and Ferry, S. 2007b. Changes in vegetation and marine environments in the eastern Mediterranean (Rhodes, Greece) during the Early and Middle Pleistocene. *Journal of the Geological Society*. 164, pp.1119–1131.

Joannin, S., Ciaranfi, N. and Stefanelli, S. 2008. Vegetation changes during the late Early Pleistocene at Montalbano Jonico (Province of Matera, southern Italy) based on pollen analysis. *Palaeogeography, Palaeoclimatology, Palaeoecology*. 270, pp.92–101.

Jobe, Z.R., Sylvester, Z., Howes, N., Pirmez, C., Parker, A., Cantelli, A., Smith, R., Wolinsky, M.A., O'Byrne, C., Slowey, N. and Prather, B. 2017. High-resolution, millennial-scale patterns of bed compensation on a sand-rich intraslope submarine fan, western Niger Delta slope. *Bulletin of the Geological Society of America*. 129, pp.23–37.

Kiro, Y., Goldstein, S.L., Garcia-Veigas, J., Levy, E., Kushnir, Y., Stein, M. and Lazar, B. 2017. Relationships between lake-level changes and water and salt budgets in the Dead Sea during extreme aridities in the Eastern Mediterranean. *Earth and Planetary Science Letters.* 464, pp.211–226.

Kirschvink, J. L. 1980. The least-squares line and plane and the analysis of palaeomagnetic data. *Geophys. J. R. Astron. Soc*. 62 pp.699–718.

Kneller, B.C., Martinsen, O.J. and McCaffrey, B. 2009. External controls on deep-water sedimentary systems: challanges and perspectives *In: External Controls on Deep-Water Depositional Systems* SEPM Special Publication No.92. (Kneller, B., Martinsen, O. and McCaffrey, B., eds.). Tulsa, OK: SEPM (Society for Sedimentary Geology), pp.5–12.

Kouli, K., Brinkhuis, H. and Dale, B. 2001. Spiniferites cruciformis: A fresh water dinoflagellate cyst? *Review of Palaeobotany and Palynology*. 113, pp.273–286.

Koymans, M.R., Langereis, C.G., Pastor-Galán, D. and van Hinsbergen, D.J.J. 2016. Paleomagnetism.org: An online multi-platform open source environment for paleomagnetic data analysis. *Computers and Geosciences*. 93 pp.127–137.

Lacey, J. H., Leng., MJ., Francke, A., Sloane, H.J., Milodowski, A., Vogel, H., Baumgarten, H., Zanchetta, G., Wagner, B. 2016. Northern Mediterranean climate since the Middle Pleistocene: a 637 ka stable isotope record from Lake Ohrid (Albania/Macedonia). *Biogeosciences* 13, pp. 1801–1820.

Leeder, M.R., Harris, T., Kirkby, M.J., and Hovius, N. 1998. Sediment supply and climate change: implications for basin stratigraphy. *Basin Research*. 10, pp.7–18.

Leeder, M.R., McNeill, L.C., Collier, R.E.L., Portman, C., Rowe, P.J., Andrews, J.E. and Gawthorpe, R.L. 2003. Corinth Rift margin uplift: new evidence from Late Quaternary marine shorelines. *Geophysical Research Letters*. 30(12), p.1611.

Leeder, M. R., Mark, D. F., Gawthorpe, R. L., Kranis, H., Loveless, S., Pedentchouk, N., Stamatakis, M. .2012. A 'Great Deepening': Chronology of rift climax, Corinth rift, Greece. *Geology*, 40, 999– 1002.

Leontaritis, A.., Kouli, K. and Pavlopoulos, K. 2020. The glacial history of Greece: a comprehensive review. *Mediterranean Geoscience Reviews*

Malartre, F., Ford, M. and Williams, E.A. 2004. Preliminary biostratigraphy and 3D geometry of the Vouraikos Gilbert-type fan delta, Gulf of Corinth, Greece. *Comptes Rendus Geoscience*. 336, pp.269–280.

Marinova, E., Harrison, S.P., Bragg, F., Connor, S., Laet, V. de, Leroy, S.A.G., Mudie, P., Atanassova, J., Bozilova, E., Carner, H., Cordova, C., Djamali, M., Filipova-Marinova, M., Gerasimenko, N., Jahns, N., Kouli, K., Kotthoff, U., Kvavadze, E., Lazarova, M., Novenko, E., Ramezani, E., Röpke, A., Shumilovskikh, L., Tanţău, I., Tonkov, S. 2018. Pollen-derived biomes in the Eastern Mediterranean–Black Sea–Caspian-Corridor. *Journal of Biogeography* 45, 484–499.

Marshall, M.H., Lamb, H.F., Huws, D., Davies, S.J., Bates, R., Bloemendal, J., Boyle, J., Leng, M.J., Umer, M. and Bryant, C. 2011. Late Pleistocene and Holocene drought events at Lake Tana, the source of the Blue Nile. *Global and Planetary Change.* 78, pp.147–161.

Marston, R.A. 2010. Geomorphology and vegetation on hillslopes: Interactions, dependencies, and feedback loops. *Geomorphology.* 116(3–4), pp.206–217.

Maslin, M.A. and Ridgwell, A.J. 2005. Mid-Pleistocene revolution and the ‘eccentricity myth’ *In*: M. Head and P. Gibbard, eds. *Early-Middle Pleistocene Transitions: The Land-Ocean Evidence. Geological Society London Special Publication No. 247.*, pp.19–34.

McArthur, A.., Kneller, B.., Wakefield, M.., Souza, P.. and Kuchle, J. 2016a. Palynofacies classification of the depositional elements of confined turbidite systems: Examples from the Gres d’Annot, SE France. *Marine and Petroleum Geology*. 77, pp.1254–1273.

McArthur, A. D., Kneller, B.C., Souza, P.A. and Kuchle, J. 2016b. Characterization of deep-marine channel-levee complex architecture with palynofacies: An outcrop example from the Rosario Formation, Baja California, Mexico. *Marine and Petroleum Geology*. 73, pp.157–173.

McArthur, Adam D., Jolley, D.W., Hartley, A.J., Archer, S.G. and Lawrence, H.M. 2016c. Palaeoecology of syn-rift topography: A Late Jurassic footwall island on the Josephine Ridge, Central Graben, North Sea. *Palaeogeography, Palaeoclimatology, Palaeoecology*. 459, pp.63–75.

McNeil, L.C., Cotterill, C.J., Henstock, T.J., Bull, J.M., Stefatos, T.J., Collier, R.E.L., Papatheoderou, G., Ferentinos, G. and Hicks, S.E. 2005. Active faulting within the offshore western Gulf of Corinth, Greece: Implications for models of continental rift deformation. *Geology*. 33, pp.241–244.

McNeill, Lisa C, Shillington, D.J., Carter, G.D.O., Everest, J.D., Gawthorpe, R.L., Miller, C., Phillips, M.P., Collier, R.E.L., Cvetkoska, A., Gelder, G. De, Diz, P., Doan, M. and Ford, M. 2019a. High-resolution record reveals climate-driven environmental and sedimentary changes in an active rift. *Scientific Reports*. 9, pp.1–11.

McNeill, L.C., Shillington, D.J., Carter, G.D.O., Everest, J.D., Le Ber, E., Collier, R.E., Cvetkoska, A., De Gelder, G., Diz, P., Doan, M.L., Ford, M., Gawthorpe, R.L., Geraga, M., Gillespie, J., Hemelsdaël, R., Herrero-Bervera, E., Ismaiel, M., Janikian, L., Kouli, K., Li, S., Machlus, M.L., Maffione, M., Mahoney, C., Michas, G., Miller, C., Nixon, C.W., Oflaz, S.A., Omale, A.P., Panagiotopoulos, K., Pechlivanidou, S., Phillips, M.P., Sauer, S., Seguin, J., Sergiou, S. and Zakharova, N.V. 2019b. Expedition 381 summary *In: Procedings of the International Ocean Discovery Program Volume 381.* IODP.

McNeill, L C, Shillington, D.J., Carter, G.D.O., Everest, J.D., Le Ber, E., Collier, R.E.L., Cvetkoska, A., De Gelder, G., Diz, P., Doan, M.L., Ford, M., Gawthorpe, R.., Geraga, M., Gillespie, J., Hemelsdaël, R., Herrero-Bervera, E., Ismaiel, M., Janikian, L., Kouli, K., Li, S., Machlus, M.L., Maffione, M., Mahoney, C., Michas, G., Miller, C., Nixon, C.W., Oflaz, S.A., Omale, A.P., Panagiotopoulos, K., Pechlivanidou, S., Phillips, M.P., Sauer, S., Seguin, J., Sergiou, S. and Zakharova, N. V 2019c. Expedition 381 methods *In: Procedings of the International Ocean Discovery Program Volume 381*. IODP.

McNeill, L.C., Shillington, D.J., Carter, G.D.O., Everest, J.D., Le Ber, E., Collier, R.E., Cvetkoska, A., De Gelder, G., Diz, P., Doan, M.L., Ford, M., Gawthorpe, R.L., Geraga, M., Gillespie, J., Hemelsdaël, R., Herrero-Bervera, E., Ismaiel, M., Janikian, L., Kouli, K., Li, S., Machlus, M.L., Maffione, M., Mahoney, C., Michas, G., Miller, C., Nixon, C.W., Oflaz, S.A., Omale, A.P., Panagiotopoulos, K., Pechlivanidou, S., Phillips, M.P., Sauer, S., Seguin, J., Sergiou, S. and Zakharova, N.V. 2019d. Site M0080 *In: Procedings of the International Ocean Discovery Program Volume 381.* IODP.

Mcneill, L.C., Shillington, D.J., Everest, J.D., Ber, E. Le, Cvetkoska, A., Gelder, G. De, Diz, P., Ford, M., Gawthorpe, R.L., Geraga, M., Gillespie, J., Ismaiel, M., Janikian, L., Kouli, K., Li, S., Machlus, M.L., Maffione, M., Mahoney, C., Michas, G., Miller, C., Nixon, C.W., Oflaz, S.A., Omale, A.P., Panagiotopoulos, K., Pechlivanidou, S., Phillips, M.P., Sauer, S., Seguin, J., Sergiou, S., Zakharova, N. V, Gulf, A., Sea, M. and Sea, A. 2019e. Site M0079 *In: Procedings of the International Ocean Discovery Program Volume 381*. IODP.

McNeill, L.C., Shillington, D.J., Carter, G.D.O., Everest, J.D., Le Ber, E., Collier, R.E., Cvetkoska, A., De Gelder, G., Diz, P., Doan, M.L., Ford, M., Gawthorpe, R.L., Geraga, M., Gillespie, J., Hemelsdaël, R., Herrero-Bervera, E., Ismaiel, M., Janikian, L., Kouli, K., Li, S., Machlus, M.L., Maffione, M., Mahoney, C., Michas, G., Miller, C., Nixon, C.W., Oflaz, S.A., Omale, A.P., Panagiotopoulos, K., Pechlivanidou, S., Phillips, M.P., Sauer, S., Seguin, J., Sergiou, S. and Zakharova, N.V. 2019f. Site M0078 *In: Procedings of the International Ocean Discovery Program Volume 381*. IDOP.

Mertens, K.N., Price, A.M. and Pospelova, V. 2012a. Determining the absolute abundance of dinoflagellate cysts in recent marine sediments II: Further tests of the Lycopodium marker-grain method. *Review of Palaeobotany and Palynology.* 184, pp.74–81.

Mertens, K.N., Rengefors, K., Moestrup, Ø., and Ellegaard, M. 2012b. A review of recent freshwater dinoflagellate cysts: taxonomy, phylogeny, ecology and palaeocology. *Phycologia.* 51, pp.612–619.

Morzadec-Kerfourn, M.T. 2005. Interaction between sea-level changes and the development of littoral herbaceous vegetation and autotrophic dinoflagellates. *Quaternary International.* 133–134, pp.137–140.

Mudie, P.J., Aksu, A.E. and Yasar, D. 2001. Late Quaternary dinoflagellate cysts from the Black, Marmara and Aegean seas: Variations in assemblages, morphology and paleosalinity. *Marine Micropaleontology*. 43, pp.155–178.

Mudie, P.J., Marret, F., Rochon, A. and Aksu, A.E. 2010. Non-pollen palynomorphs in the Black Sea corridor. *Vegetation History and Archaeobotany.* 19, pp.531–544.

Mudie, P.J., Marret, F., Mertens, K.N., Shumilovskikh, L. and Leroy, S.A.G. 2017. Atlas of modern dinoflagellate cyst distributions in the Black Sea Corridor: from Aegean to Aral Seas, including Marmara, Black, Azov and Caspian Seas. *Marine Micropaleontology*. 134, pp.1–152.

Muntzos, T. 1992. Palyno– und Paläoklima-Stratigraphie der pliozänen und altpleistozänen Sedimente der nördlichen und nordwestli- chen Peloponnes. *Newsletters on Stratigraphy*. 27, pp.71–91.

Muravchik, M., Gawthorpe, R.L., Sharp, I.R., Rarity, F. and Hodgetts, D. 2018. Sedimentary environment evolution in a marine hangingwall dipslope setting. El Qaa Fault Block, Suez Rift, Egypt. *Basin Research*. 30. pp. 452-478.

Nelson, C.., Escutia, C., Goldfinger, C., Karabanov, E., Gutierrez-Pastor, J. and De Batist, M. 2009. External Controls on Modern Clastic Turbidite Systems: Three Case Studies In: B. Kneller, O. Martinsen and B. McCaffrey, eds. *External Controls on Deep-Water Depositional Systems SEPM Special Publications*. No. 92. Tulsa, OK: SEPM (Society for Sedimentary Geology), pp.57–76.

Nguyen, N., Duffy, B., Shulmeister, J. and Quigley, M. 2013. Rapid Pliocene uplift of Timor. *Geology.* 41, pp.179–182.

Nixon, C.W., McNeill, L.C., Bull, J.M., Bell, R.E., Gawthorpe, R.L., Henstock, T.J., Christodoulou, D., Ford, M., Taylor, B., Sakellariou, D., Ferentinos, G., Papatheodorou, G., Leeder, M.R., Collier, R.E.L.I., Goodliffe, A.M., Sachpazi, M. and Kranis, H. 2016. Rapid spatiotemporal variations in rift structure during development of the Corinth Rift, central Greece. *Tectonics.* 35, pp.1225–1248.

Nyberg, B., Helland-Hansen,W., Gawthorpe, R.L., Sandbakken, P., Haug Eide, C., Sømme,T., Hadler-Jacobsen, F., Leiknes, S. 2018. Revisiting morphological relationships of modern source-to-sink segments as a first-order approach to scale ancient sedimentary systems. *Sedimentary Geology*. 373 pp. 111-133

Okuda, M., Yasuda, Y. and Setoguchi, T 2008. Middle to Late Pleistocene vegetation history and climatic changes at Lake Kopais, Southeast Greece. *Boreas*. 30 (1). pp. 73-82.

Ogg, J.G. 2020. Chapter 5 – Geomagnetic Polarity Time Scale *in* Gradstein, F., Ogg, J.G., Schmitz, M.D., Ogg, G.M eds. Geologic Time Scale 2020 (1) pp 159-192. *Elsevier*.

Panagiotopoulos, K., Holtvoeth, J., Kouli, K., Marinova, E., Francke, A., Cvetkoska, A., Jovanovska, E., Lacey, J.H., Lyons, E.T., Buckel, C., Bertini, A., Donders, T., Just, J., Leicher, N., Leng, M.J., Melles, M., Pancos, R.D., Sadori, L., Tauber, P., Vogel, H., Wagner, B. and Wilke,T. 2020. Insights into the evolution of the young Lake Ohrid ecosystem and vegetation succession from a southern European refugium during the Early Pleistocene. *Quaternary Science Reviews*. 227.

Papadopoulou, P., Iliopoulos, G., Zidianakis, I. and Tsoni, M. 2018. Vegetation and palaeoclimatic reconstruction of the Sousaki Basin (eastern Gulf of Corinth , Greece) during the Early Pleistocene. *Quaternary International.* 476, pp.110–119

Papadopoulos, G.A. 2003. Tsunami hazard in the Eastern Mediterranean: Strong earthquakes and tsunamis in Cyprus and the Levantine Sea. *Natural Hazards.* 40(3), pp.503–526.

Paropkari, A.L., Prakash Babu, C. and Mascarenhas, A. 1992. A critical evaluation of depositional parameters controlling the variability of organic carbon in Arabian Sea sediments. *Marine Geology.* 107(3).

Pechlivanidou, S., Cowie, P.A., Hannisdal, B., Whittaker, A.C., Gawthorpe, R.L., Pennos, C. and Riiser, O.S. 2018. Source-to-sink analysis in an active extensional setting: Holocene erosion and deposition in the Sperchios rift, central Greece. *Basin Research*. 30, pp.522–543.

Pechlivanidou, S., Cowie, P.A., Duclaux, G., Nixon, C.W., Gawthorpe, R.L. and Salles, T. 2019. Tipping the balance: Shifts in sediment production in an active rift setting. *Geology*. 47, pp.259–262.

Piper, D.J.W. 2006. Sedimentology and tectonic setting of the Pindos Flysch of the Peloponnese, Greece *in*: Robertson, A.H.F and Mountrakis, D (eds.) *Tectonic Development of the Eastern Mediterranean Region*, *Geological Society of London Special Publication No. 260.* Geological Society of London, pp. 493-505.

Pope, R.J., Hughes, P.D. and Skourtsos, E. 2017. Glacial history of Mt Chelmos, Peloponnesus, Greece *In*: Hughes, P.D & Woodward, J.C eds. *Quaternary Glaciation in the Mediterranean Mountains, Geological Society of London Special Publication No 433.* Geological Society of London, pp.211–236.

Posamentier, H.W. and Vail, P.R. 1988. Eustatic controls on clastic deposition II: sequence and systems tract models In: C. K. Wilgus, B. S. Hastings, H. Posamentier, J. Van Wagoner, C. A. Ross and C. G. S. C. Kendall, eds. *Sea-level changes: an integrated approach. SEPM Special Publication No.42.* SEPM, Tulsa, OK pp.125–154.

Prentice, C., Guiot, J., Huntley, B., Jolly, D., Cheddadi, R. 1996. Reconstructing biomes from palaeoecological data: a general method and its application to European pollen data at 0 and 6 ka. *Climate Dynamics*. 12. pp 185-194.

Rohais, S. and Moretti, I. 2017. Structural and Stratigraphic Architecture of the Corinth Rift (Greece): An Integrated Onshore to Offshore Basin-Scale Synthesis *In:* F. Roure, A. A. Amin, S. Khomsi and M. A. Al Garni, eds. *Lithosphere Dynamics and Sedimentary Basins of the Arabian Plate and Surrounding Areas.* Springer International Publishing, Frontiers in Earth Sciences, pp.89–120.

Rohais, S., Eschard, R., Ford, M., Guillocheau, F. and Moretti, I. 2007a. Stratigraphic architecture of the Plio-Pleistocene infill of the Corinth Rift: Implications for its structural evolution. *Tectonophysics.* 440, pp.5–28.

Rohais, S., Joannin, S., Colin, J.P., Suc, J.P., Guillocheau, F. and Eschard, R. 2007b. Age and environmental evolution of the syn-rift fill of the southern coast of the gulf of Corinth (Akrata-Derveni region, Greece). *Bulletin de la Societe Geologique de France*. 178(3), pp.231–243.

Rohais, S., Eschard, R. and Guillocheau, F. 2008. Depositional model and stratigraphic architecture of rift climax Gilbert-type fan deltas (Gulf of Corinth, Greece). *Sedimentary Geology*. 210, pp.132–145.

Romans, B.W., Castelltort, S., Covault, J.A., Fildani, A. and Walsh, J.P. 2016. Environmental signal propagation in sedimentary systems across timescales. *Earth-Science Reviews.* 153, pp.7–29.

Rovere, A., Stocchi, P. and Vacchi, M. 2016. Eustatic and Relative Sea Level Changes. *Current Climate Change Reports*. 2(4), pp.221–231.

Rubi, R., Rohais, S., Bourquin, S., Moretti, I. and Desaubliaux, G. 2018. Processes and typology in Gilbert-type delta bottomset deposits based on outcrop examples in the Corinth Rift. *Marine and Petroleum Geology*. 92, pp.193–212.

Sømme, T.O., Helland-Hansen, W., Martinsen, O.J., Thurmond, J.B. 2009. Relationships between morphological and sedimentological parameters in source-to-sink systems: a basis for predicting semi-quantitative characteristics in subsurface systems. *Basin Research*. 21 (4). pp. 361-387

Sømme, T.O., Piper, D.J.W., Deptuck, M.E., Helland-Hansen, W. 2011. Linking Onshore-Offshore Sediment Dispersal In the Golo Source-To-Sink System (Corsica, France) During the Late Quaternary. *Journal of Sedimentary Research.* 81. pp. 118-137.

Sømme, T.O., Skogseid, J., Embry, P. and Løseth, H. 2019. Manifestation of Tectonic and Climatic Perturbations I Deep-Time Stratigraphy – An Example From the Paleocene Succession offshore Western Norway. *Frontiers in Earth Science.* 7:303.

Sadori, L., Koutsodendris, A., Panagiotopoulos, K., Masi, A., Bertini, A., Combourieu-Nebout, N., Francke, A., Kouli, K., Joannin, S., Mercuri, A.M., Peyron, O., Torri, P., Wagner, B., Zanchetta, G., Sinopoli, G. and Donders, T.H. 2016. Pollen-based paleoenvironmental and paleoclimatic change at Lake Ohrid (south-eastern Europe) during the past 500 ka. *Biogeosciences*. 13 (5). pp.1423–1437.

Schmid, M., Ehlers, T.A., Werner, C., Hickler, T. and Fuentes-Espoz, J.-P. 2018. Effect of changing vegetation and precipitation on denudation-Part 2: Predicted landscape response to transient climate and vegetation cover over millennial to million-year timescales. *Earth Surface Dynamics*. 6, pp.859–881.

Sergiou, S., Beckers, A., Geraga, M., Papatheodorou, G., Iliopoulos, I. and Papaefthymiou, H. 2016. Recent Sedimentary Processes in the Western Gulf of Corinth, Greece: Seismic and Aseismic Turbitides. *Bulletin of the Geological Society of Greece*. 50, pp.383–391.

Simpson, G. and Castelltort, S. 2012. Model shows that rivers transmit high-frequency climate cycles to the sedimentary record. *Geology.* 40(12), pp.1131–1134.

Singer, B. 2014. A quatnerary geomagnetic instability time scale. *Quaternary Geochronology*. 21. pp. 29-52.

Skourtsos, E. and Kranis, H. 2009. Structure and evolution of the western Corinth Rift , through new field data from the Northern Peloponnesus *In:* U. Ring and B. Wernicke, eds. *Geological Society, London, Special Publication 321. Extending a Continent: Architecture, Rheology and Heat Budget.* pp.119–138.

Skourtsos, E., Kranis, H., Zambetakis-Lekkas, A., Gawthorpe, R.. and Leeder, M.. 2016. Alpine Basement Outcrops at Northern Peloponnesus: Implications for the Early Stages in the Evolution of the Corinth Rift. *Bulletin of the Geological Society of Greece*. 50, pp.153–163.

Smith, G.W., Nance, R.D. and Genes, A.N. 1997. Quaternary glacial history of Mount Olympus, Greece. *Bulletin of the Geological Society of America*. 109, pp.809–824.

Somerville, D.J.P., Mountney, N.P., Colombera, L., Collier, R.E.Ll. 2020. Impact of a pre-existing transverse drainage system on active rift stratigraphy: An example from the Corinth Rift, Greece. *Basin Research*. 30, *pp.* 764-788.

Stockmarr, J. 1971. Tablets with spores used in absolute pollen analysis. *Pollen et Spores*. XIII(January 1971), pp.615–621.

Strachan, L.J., Rarity, F., Gawthorpe, R.L., Wilson, P., Sharp, I. and Hodgetts, D. 2013. Submarine slope processes in rift-margin basins, Miocene Suez Rift, Egypt. *Bulletin of the Geological Society of America*. 125, pp.109–127.

Straub, K., Duller, R.A., Foreman, B.Z., Hajek, E.A. 2020. Buffered, Incomplete, and Shredded: The Challenges of Reading an Imperfect Stratigraphic Record. *Journal of Geophysical Research: Earth Surface*. 125 (3), e2019JF005079.

Suc, J.P. and Popescu, S.M. 2005. Pollen records and climatic cycles in the North Mediterranean region since 2.7 Ma In: M. . Head and P. L. Gibbard, eds*. Early-Middle Pleistocene Transitions: The Land-Ocean Evidence. Geological Society London Special Publication No. 247.* Geological Soceity London, pp.147–158.

Symeonidis, N., Theodorou, G., Schutt, H. and Veleitzelos, E. 1987. Paleontological and stratigraphic observationsin the area of Achaia and Etoloakarnania (W.Greece). *Annales Geologiques de Pays Helleniques*. 38, pp.317–353.

Szczepanek, K., Myszkowska, D., Worobiec, E., Piotrowicz, K., Ziemianin, M. and Bielec-Bąkowska, Z. 2017. The long-range transport of Pinaceae pollen: an example in Kraków (southern Poland). *Aerobiologia*. 33, pp.109–125.Taylor, B., Weiss, J.R., Goodliffe, A.M., Sachpazi, M., Laigle, M. and Hirn, A. 2011. The structures, stratigraphy and evolution of the Gulf of Corinth rift, Greece. *Geophysical Journal International.* 185, pp.1189–1219.

Taylor, B., Weiss, J.R., Goodliffe, A.M., Sachpazi, M., Laigle, M. and Hirn, A. 2011. The structures, stratigraphy and evolution of the Gulf of Corinth rift, Greece. *Geophysical Journal International*. 185(3) pp.1189–1219.

Tofelde, S., Bernhardt, A., Guerit, L. and Romans, B.W. 2021. Times Associated With Source-to-Sink Propagation of Environmental Signals During Landscape Transience. *Frontiers in Earth Science: Sedimentology, Stratigraphy and Diagenesis* 9:628315. doi: 10.3389/feart.2021.628315

Torfstein, A., Goldstein, S.L., Stein, M. and Enzel, Y. 2013. Impacts of abrupt climate changes in the Levant from Last Glacial Dead Sea levels. *Quaternary Science Reviews*. 69, pp.1–7.

Toucanne, S., Zaragosi, S., Bourillet, J.F., Dennielou, B., Jorry, S.J., Jouet, G. and Cremer, M. 2012. External controls on turbidite sedimentation on the glacially-influenced Armorican margin (Bay of Biscay, western European margin). *Marine Geology.* 303–306, pp.137–153.

Trenberth, K.E., Dai, A., Rasmussen, R.M. and Parsons, D.B. 2003. The changing character of precipitation. *Bulletin of the American Meteorological Society*. 84(9), pp.1205-1217+1161.

Tucker, G.E., McCoy, S.W., Whittaker, A.C., Roberts, G.P., Lancaster, S.T. and Phillips, R. 2011. Geomorphic significance of postglacial bedrock scarps on normal-fault footwalls. *Journal of Geophysical Research: Earth Surface.* 116(1), pp.1–14.

Tyson, R.. 1995. Sedimentary Organic Matter: Organic facies and palynofacies. *Chapman & Hall*, London.

Tzedakis, P.C., Hooghiemstra, H. and Pälike, H. 2006. The last 1.35 million years at Tenaghi Philippon: revised chronostratigraphy and long-term vegetation trends. *Quaternary Science Reviews*. 25, pp.3416–3430.

Vidal, G. 1988. American Association of Stratigraphic Palynologists A Palynological Preparation Method Stratigraphic Palynologists. *Palynology*. 12, pp.215–220.

Wagner, B., Vogel, H., Francke, A., Friedrich, T., Donders, T., Lacey, J.H., Leng, M.J., Regattieri, E., Sadori, L., Wilke, T., Zanchetta, G., Albrecht, C., Bertini, A., Combourieu-Nebout, N., Cvetkoska, A., Giaccio, B., Grazhdani, A., Hauffe, T., Holtvoeth, J., Joannin, S., Jovanovska, E., Just, J., Kouli, K., Kousis, I., Koutsodendris, A., Krastel, S., Lagos, M., Leicher, N., Levkov, Z., Lindhorst, K., Masi, A., Melles, M., Mercuri, A.M., Nomade, S., Nowaczyk, N., Panagiotopoulos, K., Peyron, O., Reed, J.M., Sagnotti, L., Sinopoli, G., Stelbrink, B., Sulpizio, R., Timmermann, A., Tofilovska, S., Torri, P., Wagner-Cremer, F., Wonik, T. and Zhang, X. 2019. Mediterranean winter rainfall in phase with African monsoons during the past 1.36 million years. *Nature.* 573, pp.256–260.

Watkins, S.E., Whittaker, A.C., Bell, R.E., McNeill, L.C., Gawthorpe, R.L., Brooke, S.A.S. and Nixon, C.W. 2018. Are landscapes buffered to high-frequency climate change? A comparison of sediment fluxes and depositional volumes in the Corinth Rift, central Greece, over the past 130 k.y. *Bulletin of the Geological Society of America.* 131, pp.372–388.

Watkins, S.E., Whittaker, A.C., Bell, R.E., Brooke, S.A.S., Ganti, V., Gawthorpe, R.L., McNeill, L.C. and Nixon, C.W. 2020. Straight from the source's mouth: Controls on field-constrained sediment export across the entire active Corinth Rift, central Greece. *Basin Research,* doi: 10.1111/bre.12444

Westaway, R. 2002. The Quarternary evolution of the Gulf of Corinth, central Greece: coupling between surface processes and flow in the lower continental crust. *Tectonophysics.* 348, pp.269–318.

Whittaker, A.C., Attal, M. and Allen, P.A. 2010. Characterising the origin, nature and fate of sediment exported from catchments perturbed by active tectonics. *Basin Research.* 22(6), pp.809–828.

Whittaker, A.C., Duller, R.A., Springett, J., Smithells, R.A., Whitchurch, A.L. and Allen, P.A. 2011. Decoding downstream trends in stratigraphic grain size as a function of tectonic subsidence and sediment supply. *Bulletin of the Geological Society of America*. 123(7–8), pp.1363–1382.

Woodward, J.C., Lewin, J. and MacKlin, M.G. 1992. Alluvial sediment sources in a glaciated catchment: The voidomatis basin, Northwest Greece. *Earth Surface Processes and Landforms.* 17(3), pp.205–216.

Yang, T., Hyodo M., Yang, Z., Fu, J., 2004. Evidence for the Kamikatsura and Santa Rosa excursions recorded in eolian deposits from the Southern Chinese Loess Plateau. *Journal of Geophysical Research: Solid Earth*. 109(12). pp. 1-10.

Zhang, J., Burgess, P.M., Granjeon, D. and Steel, R. 2019a. Can sediment supply variations create sequences? Insights from stratigraphic forward modelling. *Basin Research*. 31, pp.274–289.

Zhang, J., Kim, W., Olariu, C. and Steel, R. 2019b. Accommodation- versus supply-dominated systems for sediment partitioning to deep water. *Geology*. 47, pp.1–4.

Zhong, X., Escalona, A., Sverdrup, E. and Bukta, K.E. 2018. Impact of fault evolution in Gilbert-type fan deltas in the Evrostini area, south-central Gulf of Corinth, Greece. *Marine and Petroleum Geology*. 95, pp.82–99.

Zobaa, M.K., Salah, Y., Taha, A.A. and Oboh-ikuenobe, F.E. 2015. Improved Graphical Representation of Sedimentary Organic Matter as Paleoenvironmental Parameters *In: GSA 2015 Conference Proceedings. Baltimore, Maryland, USA,* 47, p.365.

11 Supplementary Information

Supplementary Data 1: Summary of samples and sample depths for G4

Supplementary Data 2: *Zidjerveld Palaeomag plots*

Supplementary Data 3: Outcrop model (hosted on V3GEO)

Supplementary Data 4: *Raw Palynology counts*

Supplementary Data 5: Biomization summary